Aerogels Containing Metal, Alloy, and Oxide Nanoparticles Embedded into Dielectric Matrices 16

Anna Corrias[a*,1] Danilo Loche[a,2] and Maria Francesca Casula[b,3]

[a] School of Physical Sciences, Ingram Building, University of Kent, Canterbury CT2 7NH, United Kingdom
[b] Department of Chemical and Geological Sciences and INSTM, University of Cagliari, S.S. 554 Bivio per Sestu, 09042, Monserrato, CA, Italy
E-mail: [1]A.Corrias@kent.ac.uk; [2]D.Loche@kent.ac.uk; [3]casulaf@unica.it

Abstract Aerogels are regarded as ideal candidates for the design of functional nanocomposites based on supported metal or metal oxide nanoparticles. The large specific surface area together with the open pore structure enables aerogels to effectively host finely dispersed nanoparticles up to the desired loading and to provide nanoparticle accessibility as required to supply their specific functionalities.

The incorporation of nanoparticles as a way to increase the possibility of the use of aerogels as innovative functional materials and the challenges in the controlled preparation of nanocomposite aerogels is reviewed in this chapter.

16.1 Introduction

Aerogels are innovative solids that have many unique optical, insulating, and catalytic properties [1]. Tailored features of aerogels can be obtained by finely tuning the composition, the surface, and the microstructure (i.e., porosity and texture, crystallinity, and grain size) of the resulting material, which are controlled by the sol–gel parameters [2].

A way to expand the potential of aerogels to provide innovative functional materials is through the design of nanocomposites, where metal or metal oxide nanoparticles are incorporated within the aerogel matrix. In addition to broadening the range and viability of aerogels, the preparation of nanocomposites provides a means of preventing nanocrystal aggregation and growth through particle confinement, fulfilling a key requirement for any practical application. Among the main features which make aerogels ideal candidates for the design of functional nanocomposites are i) the large specific surface area, and ii) the occurrence of an open and interconnected pore structure. While an extended surface area enables to host effectively finely dispersed nanophases up to high loadings, the open porosity ensures nanoparticle accessibility, as required to carry out their specific functionalities.

Despite a considerable amount of progress has been reached in the field of aerogel nanocomposites, major challenges remain in the control of the homogeneity, loading, size, and distribution of the nanoparticles within the host inorganic network, i.e. all the parameters which directly determine the electronic, optical, magnetic, and catalytic properties of nanocomposite materials.

A major issue is related to the difference in chemical properties of the precursors for the nanophase (usually metal salts) and for the inorganic matrix (commonly alkoxides), as many sol–gel process parameters influence the hydrolytic poly-condensation of each precursor differently [3].

Although this is a general problem in the design of any sol–gel nanocomposite, it is more critical in the case of aerogels, which require the original solvent present in the gel (usually ethanol or methanol in alcogels and water in aquogels), to be replaced by solvent exchange and then removed by supercritical solvent extraction. The supercritical drying step will be hereafter named *sc-HT* or *sc-CO_2 drying* depending on whether alcohols or carbon dioxide are supercritically evacuated (requiring typical temperatures of ~350 and 40°C respectively). This step introduces additional issues concerning solubility of the precursors and thermal stability under the supercritical drying conditions.

The different strategies that have been adopted to synthesize nanocomposite aerogels follow two general approaches, depending on whether the nanophase (or its precursor) is added during or after the sol–gel process.

The first approach includes co-hydrolysis and co-gelation of the nanoparticle and of the matrix precursors and co-gelation of the matrix precursor together with preformed nanoparticles. This approach offers the advantage of producing materials with a controllable loading of nanoparticles throughout. On the other hand, several disadvantages should be taken into account: an accurate choice of the synthetic conditions has to be made in order to obtain a homogeneous multicomponent gel, and the nanoparticle precursors as well as the capping agents needed to stabilize preformed colloidal nanoparticles may affect the sol–gel synthesis of the matrix.

The second approach includes methods based on the addition of the nanophase after the sol–gel process and they should preserve the porous structure and morphology of the matrix. These methods include the deposition of the nanophase by impregnation, deposition–precipitation, and chemical vapor infiltration procedures. Deposition–precipitation synthesis, based on the deposition of metal hydroxides on the support by tuning the pH of the solution, as well as impregnation of a preformed aerogel by a solution of metal salts, are very straightforward and inexpensive routes. These approaches, however, suffer from two major drawbacks: (1) the poor compositional homogeneity of the resulting nanocomposites and (2) the potential damage of the support in liquid media, aerogels being brittle and fragile. Tethering the metal to a gel matrix modified by coordinating groups and soaking the alcogel or aquogel into the metal solution prior to supercritical drying have been proposed as a way to overcome respectively drawbacks described in (1) and (2).

Deposition of nanoparticles from vapor phase, as opposed to wet impregnation methods, does not alter the porous matrix and ensures that the guest phase will be distributed throughout the matrix, thanks to its open porous texture. The general applicability of this approach is limited by the availability of precursors with a sufficiently high vapor pressure to give rise to volatile by-products.

Figure 16.1 is a schematic summary of the different preparation approaches; it should be taken into account, however, that a post-synthesis treatment, most commonly a thermal treatment under controlled atmosphere, is required to induce phase separation, to promote the formation of the desired oxide or metallic nanophase, and to obtain the desired crystallinity, as will be discussed later.

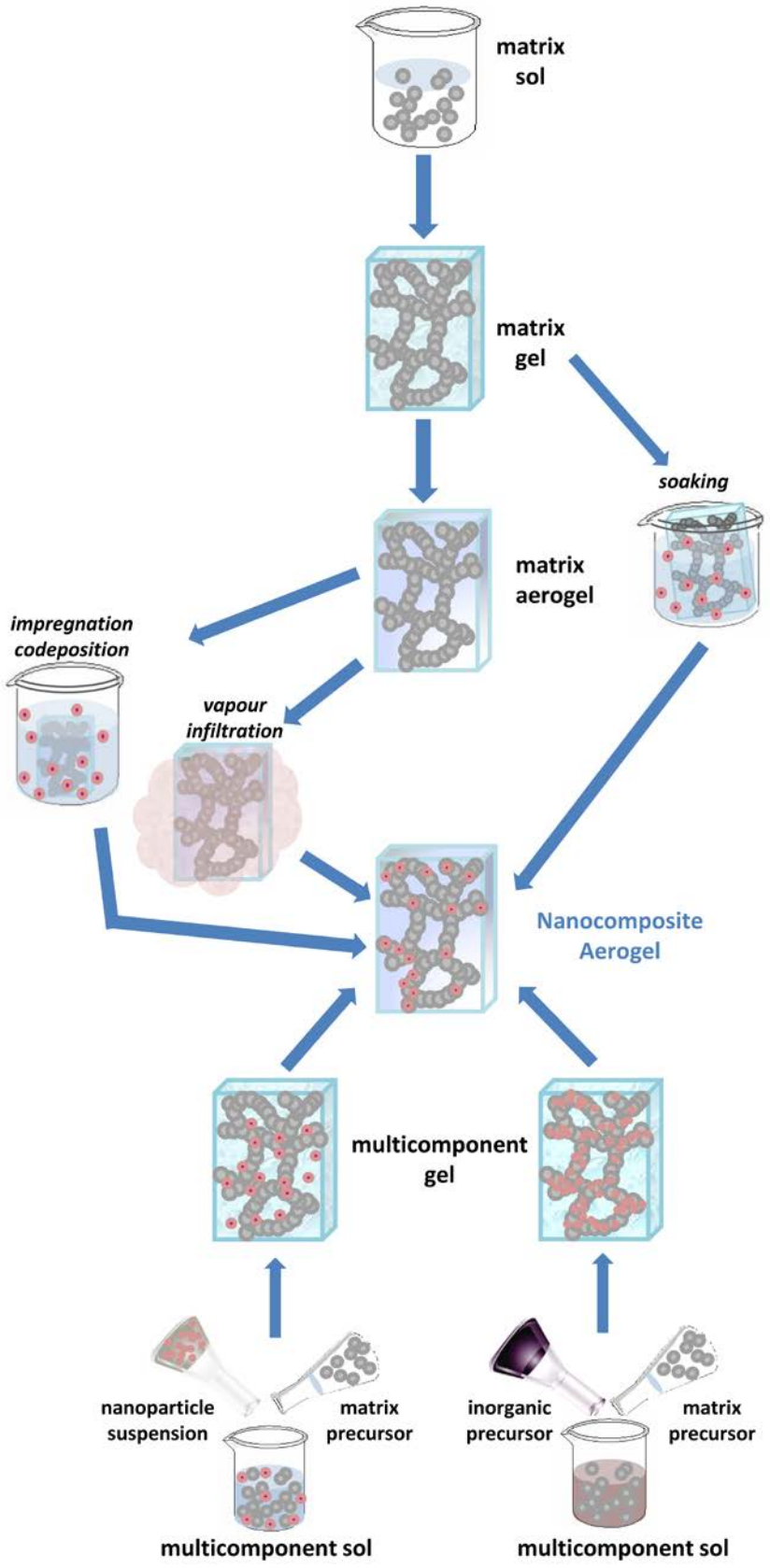
matrix sol
matrix gel
soaking
matrix aerogel
impregnation codeposition
vapour infiltration
Nanocomposite Aerogel
multicomponent gel
nanoparticle suspension
matrix precursor
multicomponent sol
inorganic precursor
matrix precursor
multicomponent sol

Figure 16.1 Schematic diagram of the different approaches for the chemical synthesis of nanocomposite aerogels.

In the following, some recent examples of nanocomposite aerogels will be reviewed with the aim of pointing out some significant advances in the preparation of functional nanocomposite aerogels made out of supported metal, alloy, or metal oxide nanoparticles dispersed in a dielectric matrix. Although we are aware that this chapter is not a comprehensive report of all the literature on nanocomposite aerogels, the aim of our overview is to highlight how the incorporation of nanoparticles may increase the possibility of using aerogels as innovative materials and how to select the most promising preparation route for obtaining nanocomposite aerogels for a given application. From the compositional point of view, the unique properties of silica aerogel matrices are still the most extensively exploited (Chap. SiO_2 Aerogels), but alternative inorganic (Part C) and polymeric (Parts D and E) matrices are now being envisaged, opening further routes for expanding the range of preparation protocols and functionalities of aerogels. Among the aerogels that are not covered by this chapter, nanocomposites based on carbon (Part G) are particularly promising for electrochemical applications such as the design of high performance electrodes [4, 5].

16.2 Aerogel Containing Oxide Nanoparticles

Several examples are available in the literature on the synthesis of aerogels containing oxide nanoparticles embedded into dielectric matrices to be used for their magnetic, catalytic, and optical properties. While almost all of the examples refer to SiO_2-based nanocomposites, a large variety of oxide nanoparticles have been synthesized as a dispersed nanophase.

16.2.1 Silica-based aerogels containing oxide nanoparticles

The synthesis of silica-based iron oxide nanocomposites has been attempted by different approaches, with the main aim to stabilize superparamagnetic iron oxide nanoparticles, mainly in the maghemite, γ-Fe_2O_3, polymorph. Although this metastable phase is frequently kinetically stable at the nanometer scale, it proved to be difficult to obtain. Indeed, the production of iron oxide-SiO_2 aerogels represents an interesting case study both because maghemite is a relevant model system for magnetic materials at the nanoscale, and because of the very rich and complex redox chemistry and polymorphism in iron oxides and oxyhydroxides.

Casas et al. [6] prepared several magnetic samples (see Figure 16.2) by exploring the role of several sol–gel parameters. In particular, different precursors for the silica (*TEOS* or *TMOS*) in alcoholic solution (ethanol or methanol) were tested in the presence of variable amounts of water and using acid or base catalyst. They also used two different iron oxide precursors: either $Fe(NO_3)_3 \cdot 9H_2O$ or a $(FeNa(EDTA) \cdot 2H_2O)$ metallic complex in order to avoid strong bonding to the matrix and to increase pore diameters. The samples obtained with these procedures have surface areas ranging between 200 and 600 $m^2\ g^{-1}$, while *XRD* does not permit a clear identification of peaks apart from one single case in which the presence of six-line ferrihydrite, a poorly crystalline iron oxide hydroxide, became apparent. Mössbauer spectroscopy allowed identification of the iron oxide phase as ferrihydrite in some samples and magnetite in others and also indicated

that the samples present *superparamagnetic relaxation* effects. *TEM* shows either spherical or acicular nanoparticles.

Mendoza et al. [7] modified this procedure for the preparation of monolithic and magnetic aerogel nanocomposites containing 6 nm size γ-Fe_2O_3 nanoparticles where *MTMS* has been used with *TEOS* in order to introduce a hydrophobic character through surface modification. Different Fe/Si mass ratios have been studied reaching surface area up to 698 $m^2\ g^{-1}$ and superparamagnetic behavior.

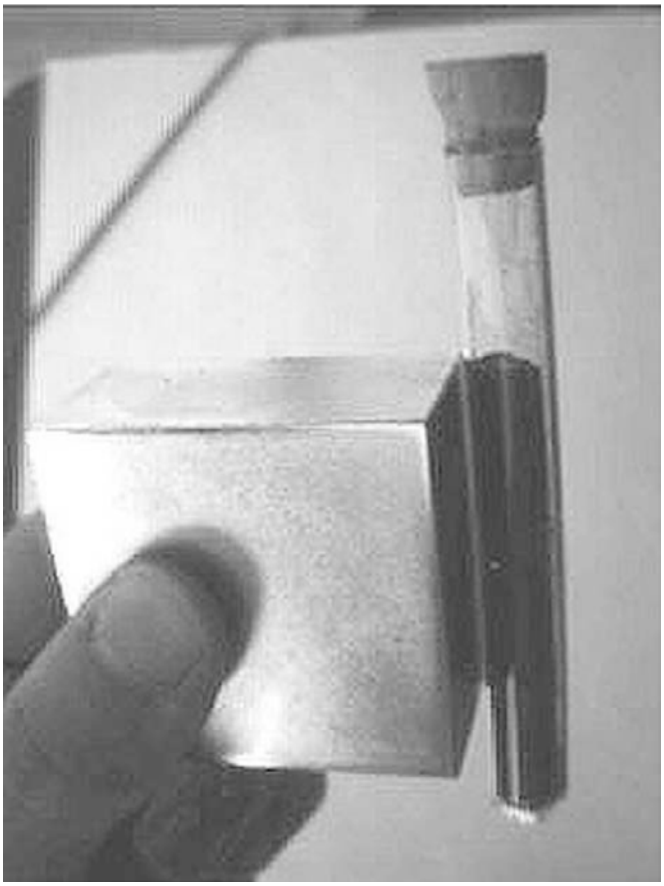

Figure 16.2 Magnetic aerogel attracted by a permanent magnet (reproduced from [6] by permission of Elsevier).

Fe_2O_3–SiO_2 nanocomposite aerogels were also prepared in the form of *microporous* and narrow *mesoporous* aerogels by *sc-HT drying* of alcogels obtained by using *TEOS* and $Fe(NO_3)_3 \cdot 9H_2O$ as precursors for the silica matrix and the iron oxide nanoparticles, respectively, while ethanol was used as solvent and nitric acid as catalyst [8]. *XRD* of the aerogels after supercritical drying showed faint peaks due to six-line ferrihydrite. After supercritical drying, samples were calcined at elevated temperatures. After calcination, new *XRD* peaks showed up and kept on growing. At 900°C, there was a mixture of different Fe(III) oxides present. Surface areas were quite high even after calcination at 900°C (500 $m^2\ g^{-1}$) and *TEM* images showed a homogeneous distribution of the nanoparticles.

Following a slightly different sol–gel method [9], in fact similar to that reported by Del Monte et al. for the preparation of xerogels [10], the same group obtained aerogels consisting of pure maghemite nanoparticles dispersed into silica. The same precursors as in [8] were used, but gelation was performed in a closed container at 50°C and *sc-HT drying* was performed using the conditions that led to *microporous* aerogels. After supercritical drying, calcination was directly performed at 400°C. The *XRD* patterns of the calcined aerogels present broad peaks due to nanocrystalline maghemite on top of the amorphous silica background. Mössbauer spectroscopy and magnetic measurements show the typical features of *superparamagnetic materials*. While this procedure was effective in producing only the desired iron oxide polymorph with high crystallinity under relatively mild conditions, *TEM* micrographs show that individual nanoparticles with a narrow distribution of size (around 4 nm) are located in large and irregular aggregates within the amorphous matrix, as shown in Figure 16.3.

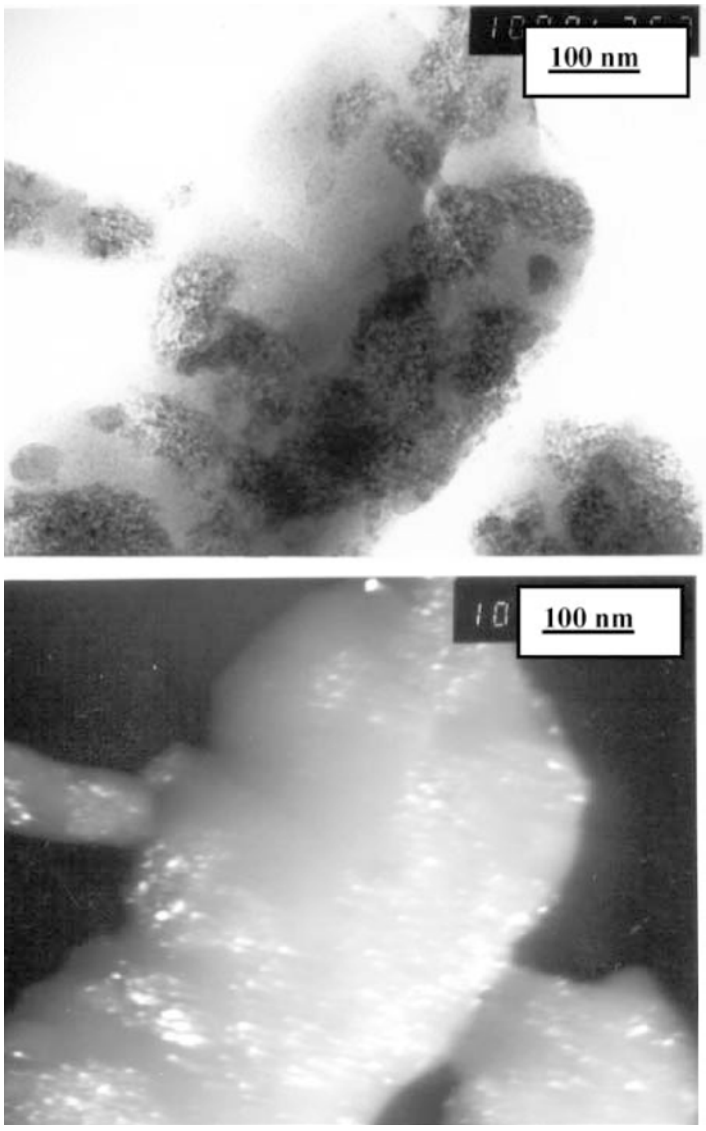

Figure 16.3 *BF* (**top**) and *DF* (**bottom**) TEM micrographs of maghemite–SiO_2 aerogel (reproduced from [9] by permission of The Royal Society of Chemistry).

Monoliths of iron oxide nanoparticles hosted in silica aerogels were prepared by Casas et al. using two different sol–gel routes [11]. In the first one, a preformed gel was soaked in an $Fe(NO_3)_3$ solution, while in the second case, all the precursors were mixed and the nanocomposite was obtained by co-gelation. *Sc-CO_2 drying* was performed and samples were then annealed in air. *XRD* patterns, shown in Figure 16.4, show the formation of maghemite nanoparticles for samples obtained by soaking the gel, while samples obtained by co-gelation show the presence of six-line ferrihydrite. Investigation of the magnetic dynamic behavior of the aerogels obtained by soaking [12] points to a *superparamagnetic behavior* without interparticle interactions, indicating that the synthetic path is effective at preventing particle aggregation.

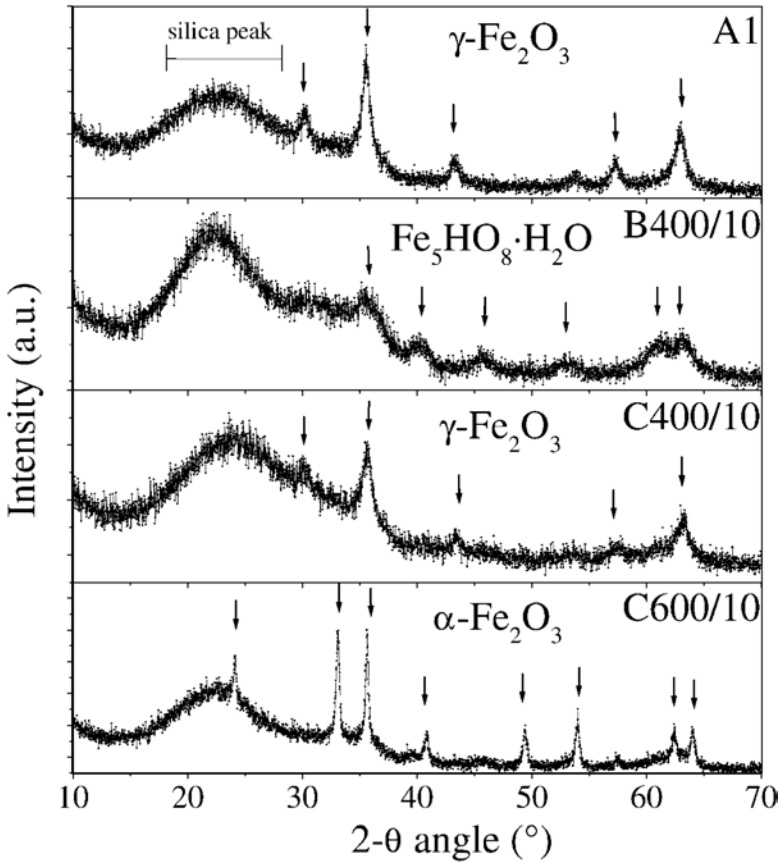

Figure 16.4 XRD patterns of iron oxide–silica aerogels obtained by soaking (A1) and by cogelation (B400) (reproduced from [11] by permission of Springer).

In order to avoid the introduction of water, iron oxide–silica aerogel nanocomposites were prepared by the same group by impregnation of wet gels [13], obtained under acidic catalysis, with either anhydrous ferrous acetate or anhydrous ferrous acetylacetonate. *XRD* shows peaks of a cubic oxide spinel phase with nanoparticle diameters around 5–6 nm, which is also confirmed by *TEM* (7–8 nm). Mössbauer confirmed that the nanoparticles consist of maghemite and the amount of that phase was estimated at 11–13% (w/w). In this case, the maghemite nanophase was formed without the need of post-annealing treatments due to the absence of water. Surface areas of the samples were around 900 $m^2\ g^{-1}$. Mössbauer spectroscopy on the aerogels obtained by impregnation of

wet gels with ferrous acetylacetonate in neutral medium [14] confirms the presence of maghemite nanoparticles (6 nm) in a nanocomposite with low apparent density (0.2 g cm^{-3}) without post-annealing.

Maghemite–silica nanocomposite aerogels were prepared by van Raap et al. using different precursors (*TEOS* and *TMOS*) and different pressure–temperature drying conditions [15]. The *XRD* patterns of the aerogels prepared with both *TEOS* and *TMOS* display weak reflection lines due to maghemite or magnetite. Mössbauer indicates that aerogels prepared using *TMOS* contain some Fe^{2+}. Those samples had also larger pores, by *TEM*.

The synthesis of high surface area, *mesoporous* iron–silicon mixed oxide aerogel was studied by Fabrizioli et al. [16] by varying different sol–gel parameters, such as gelation agents (*N*,*N*-diethylaniline, trihexylamine, $(NH_4)_2CO_3$, or NH_3), concentration of iron precursor ($Fe(NO_3)_3 \cdot 9H_2O$), type of silicon precursor (*TMOS* or *TEOS*), and post-annealing treatment. In most cases, transparent gels are obtained, whereas $(NH_4)_2CO_3$ gives rise to hazy gels. *Sc-CO_2 drying* is followed by annealing first under flowing N_2 up to 200°C and then in air first at 200°C and then at 600°C. After calcination at 600°C, all aerogels were amorphous by *XRD* and *TEM*. Samples further calcined at 900°C showed a broad reflection, which was attributed to either maghemite or magnetite nanocrystals. EPR shows different iron species: isolated tetrahedrally coordinated iron, iron oxide clusters, and superparamagnetic iron oxide clusters of increasing size with the iron loading.

Maleki et al. [17] explored a new way to prepare an aerogel nanocomposite employing magnetite nanoparticles with a thin silica layer in order to increase the compatibility of the pre-synthesized magnetic phase with the silica matrix. The authors modified their synthesis [18] for silica aerogel-like monoliths by ambient pressure drying (APD) and by cross-linking the silica surface with triacrylate cross-linker in order to improve the mechanical properties. The nanocomposite showed an increase in the compressive strength and an improvement of the thermal insulation performance with a slight decrease in the active surface area compared to the un-doped material. Moreover, no influence on hydrophobicity has been observed.

Mixed oxide nanocomposites in which iron(III) oxide is the major component and silica is the minor component were prepared by Clapsaddle et al. [19] using $FeCl_3 \cdot 6H_2O$ with either *TMOS* or *TEOS* in the presence of an organic epoxide as gelling agent (propylene oxide, PO, or trimethylene oxide, TMO) with Fe/Si molar ratios varying between 1 and 5. Drying was performed using *sc-CO_2*. This is an extension of the use of organic epoxides (Chap. A Robust Approach to Inorganic Aerogels: The Use of Epoxides in Sol-Gel Synthesis) for the preparation of metal oxides [20], giving rise to the formation of aerogel monoliths, as shown in Figure 16.5. In order to obtain homogeneous sols, the iron salt was dissolved in ethanol and partially reacted with the epoxide promoter before addition of *TEOS* or *TMOS*. The composites contain an iron(III) phase, which was not clearly identified, and silica. The *FTIR* results suggest the iron oxide phase to be an iron oxide hydroxide due to the presence of water and hydroxyl groups. The most pronounced effect on gelation times comes from the epoxide used; a minor influence was also observed from the Fe/Si ratio and the silica precursor. All the materials had surface areas between 350 and 450 m^2 g^{-1} and were *mesoporous*. *TEM* showed that the *mesoporous* structure was due to a collection of nanoparticles clustered

together, particle size depending on the epoxide used (bigger particles with *TMOS*). Elemental maps indicate that Fe and Si are uniformly dispersed.

Wang et al. [21] tested mesoporous silica aerogels containing nanoparticles of different ferric species as catalysts for partial oxidation of methanol. A two-stage sol-gel procedure has been employed to prepare nanocomposites containing 0.5-20 wt% of Fe_2O_3 using ferric acetylacetonate and *TEOS* as precursors and methanol as solvent, followed by *sc-HT drying*. The materials have large surface areas of 764-870 $m^2\ g^{-1}$. The iron oxide phase identification was not possible due to the absence of crystalline peaks in the *XRD* patterns that the authors attribute to the small dimension of the nanoparticles (1–5 nm as shown by *TEM* analysis). The nanocomposites are catalytically active and selective to formaldehyde and methyl formate production.

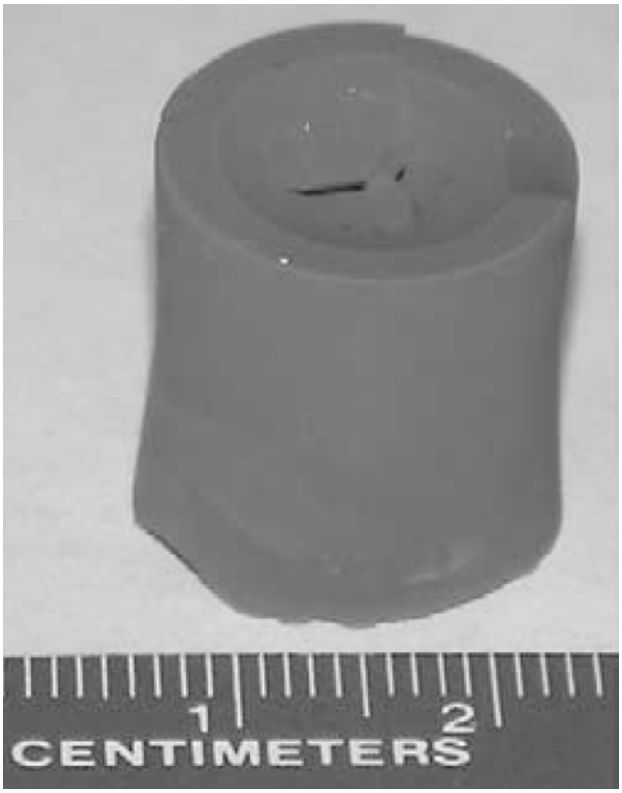

Figure 16.5 Photograph of a Fe/Si = 1 aerogel monolith (reproduced from [19] by permission of Elsevier).

Several other silica-based aerogels containing transition metal oxides have also been prepared. Casula et al. [22] prepared NiO–SiO_2 nanocomposite aerogels using *TEOS* and $Ni(NO_3)_2 \cdot 6H_2O$ as precursors for the silica matrix and for the NiO nanoparticles, respectively, ethanol as solvent and nitric acid as catalyst. By adopting four different *sc-HT drying* procedures that differ in the heating ramp, the solvent used to fill the autoclave, and the initial overpressure in the autoclave, *mesoporous* or *microporous* aerogels were obtained. The *XRD* of the aerogels showed peaks due to $Ni(NO_3)_2Ni(OH)_2$ and $Ni(OH)_2$. Upon calcination at 773 K, high surface areas were retained (500–900 $m^2\ g^{-1}$), while the porosity of the samples varied depending on the supercritical drying

conditions. *XRD* shows peaks due to NiO nanocrystals and *TEM* showed that crystal size varied between 2 and 10 nm depending on the porosity of the host aerogel matrix.

Selected $NiO–SiO_2$ aerogels were tested [23] as catalysts for the nitroxidation of hydrocarbons and compared to the corresponding xerogels and to Ni-composites based on an alumina matrix. The structural and textural features of the materials were investigated by *XRD* and *TEM* and combined to the acid/base and reducibility data as deduced by adsorption microcalorimetry and *TPR* profiles. A relevant feature of alumina is that, as opposed to amorphous silica, it is nanocrystalline under these conditions. The alumina-based samples are made out of nanocrystalline nickel aluminate and are mesoporous, where the aerogel has larger pore volumes and surface area than the xerogel. On the other hand, in the silica-based samples nickel oxide nanocrystals form within the amorphous silica, the size of the nanocrystals being around 5 nm in the microporous xerogel and 14 nm in the mainly mesoporous aerogel. *TPR* data point out that the alumina based samples have similar reducibility, whereas significant differences were observed in the silica-supported composites, the $NiO–SiO_2$ aerogel exhibiting improved reducibility at low temperature. The NO-catalyst interaction was monitored by temperature programmed NO reaction coupled to mass spectrometry and preliminary tests on the use of the $NiO–SiO_2$ xerogel and aerogel nanocomposites for the catalytic nitroxidation of 1-methylnaphthalene to 1-naphthonitrile were obtained in a fixed bed continuous-flow reactor. The data indicate that the aerogel exhibits larger selectivity than the corresponding xerogel, pointing out the textural characteristics of aerogels play an essential role in the design of porous composite materials for catalytic applications.

Another example of prospective catalysts which are of interest in the field of fuel cells related industrial processes is provided by copper-based silica aerogels. Here, copper is regarded as a cost-effective alternative to catalytically active noble metals and a key role in the catalytic performance is related to its redox chemistry. Indeed, while zero-valent copper might form during the industrial process and can be regarded as the active phase, the starting catalyst contains a copper oxide phase.

The production of a copper-based silica aerogel has been achieved from $Cu(NO_3)_2 \cdot 3H_2O$ and sodium silicate. The gel was submitted to solvent exchange and drying control chemical additive (DCCA) processing with hexamethyldisilazane and then the aerogel was produced by gradual calcination [24]. The produced composites are made out of a mixture of CuO and minor copper-silicate phases dispersed into amorphous silica, and resulted to be active in the H_2 production from methanol reforming. In particular, a much higher selectivity was observed in the aerogel as compared to a commercial catalyst (Figure 16.6).

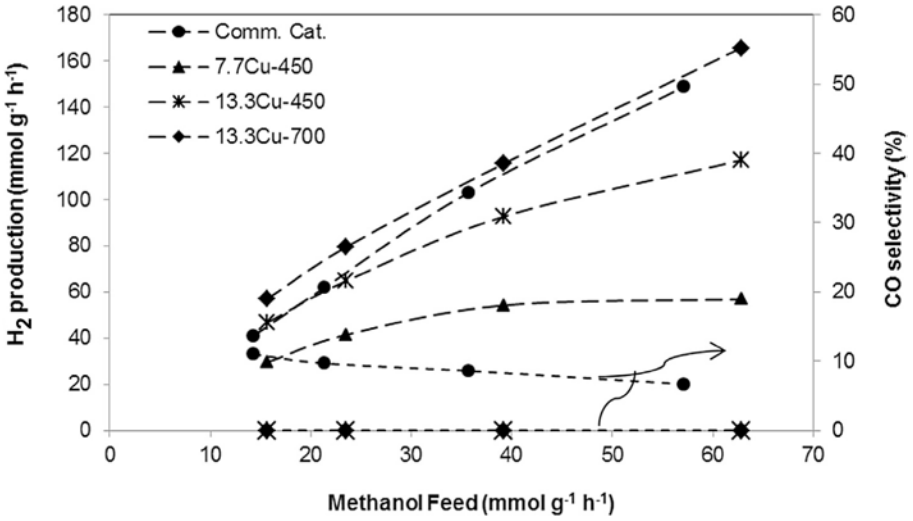

Figure 16.6 Catalytic activity and selectivity of Cu-SiO_2 aerogel catalysts with different copper weight percent (7.7 and 13.3%) and calcination temperature (450 and 700°C) compared with a CuO/ZnO/Al_2O_3 commercial catalyst (reproduced from [24] by permission of Elsevier).

Marras et al. [25] investigated copper-based nanoparticles, supported on either a silica aerogel or cubic mesostructured silicas as catalysts for the water gas shift reaction. The obtained nanocomposites were characterised before and after catalysis through N_2 physisorption measurements, *TEM* and *XRD*. The samples before catalysis contained nanoparticles of copper oxides (either CuO or Cu_2O), whereas the formation of metallic copper nanoparticles, constituting the active catalytic phase, was observed either by using pre-treatment in a reducing atmosphere or directly during the catalytic reaction owing to the presence of carbon monoxide. A key role in determining the catalytic performances of the samples is played by the ability of different matrices to promote a high dispersion of copper metal nanoparticles. The best catalytic performances are obtained with the aerogel sample, which also exhibits constant carbon monoxide conversion values at constant temperature and reproducible behaviour after subsequent catalytic runs.

Nanoparticles of ZnO were introduced into the pores of a preformed SiO_2 aerogel by immersion in a dilute aqueous solution of $ZnSO_4 \cdot 7H_2O$ [26], followed after a few days by addition of NH_3, which caused precipitation of $Zn(OH)_2$. Finally, thermal treatment was performed at temperatures varying between 200 and 1,150°C. *XRD* indicated the presence of ZnO with particle size increasing with the temperature of the thermal treatment. The photoluminescence intensities of the nanocomposites at about 500 nm were 10–50 times higher than that of bulk nanostructured ZnO, depending on the conditions of the thermal treatment.

Amlouk et al. [27] incorporated TiO_2 nanopowder in a silica aerogel. The nanopowder was prepared by the sol–gel process using titanium (IV) isopropoxide in a mixture of methanol and acetic acid. The nanopowder was mixed with *TEOS* and water, while ethanol and HF were used as the solvent and catalyst, giving rise to instantaneous gel formation. The gel was submitted to *sc-HT drying* and the aerogel was annealed at 1,200°C. *XRD* showed small peaks due to rutile on top of the amorphous silica background. The crystallite size was determined to be 20 nm for sample annealed at 523

K and 300 nm for sample annealed at 1,473 K. Those nanocomposites exhibited a strong near-infrared luminescence band centered at about 850 nm.

The same group prepared in a very similar way samples of silica aerogels incorporating an Al_2O_3 nanopowder [28]. *XRD* of samples annealed at 1,150°C showed the presence of peaks due to α-Al_2O_3 and δ-Al_2O_3. The crystallite size of samples annealed at 700°C was estimated at 30 nm. Photoluminescence spectra showed strong luminescent bands at about 500 and 770 nm. Other nanopowders such as ZnO and SnO_2 have been also incorporated, producing strong luminescence bands in the same regions [29].

Tin oxide nanocrystals were incorporated in the *mesoporous* network of a silica aerogel also by Wei et al. [30]. In this case, silica aerogel was obtained via ambient pressure drying after multiple surface modifications with trimethylchlorosilane. Before surface modification ethanol was replaced with *n*-hexane, which is a suitable solvent for trimethylchlorosilane and for ambient pressure drying because of its low surface tension. The deposition of tin oxide nanocrystals was achieved by immersing the aerogel first in an aqueous solution of $SnCl_4$ and then in an aqueous solution of NH_3. Annealing was required to form the oxide nanoparticles. The aerogel nanocomposite had a much lower surface area than the original silica aerogel, as expected. Moreover, after the incorporation of the nanoparticles the pores lost their well-defined size and shape. *HREM* images of samples treated at 400°C showed several tin oxide nanocrystals with interlayer spacings in three different directions and some evidence of dislocation and vacancy clustering. The composite aerogels exhibit a rich photoluminescence and promising photocatalytic ability toward photodegradation of methylene blue, as shown in Figure 16.7 where conversion before and after UV exposure for the nanocomposite aerogel treated at 500°C is compared with that of a pure silica aerogel.

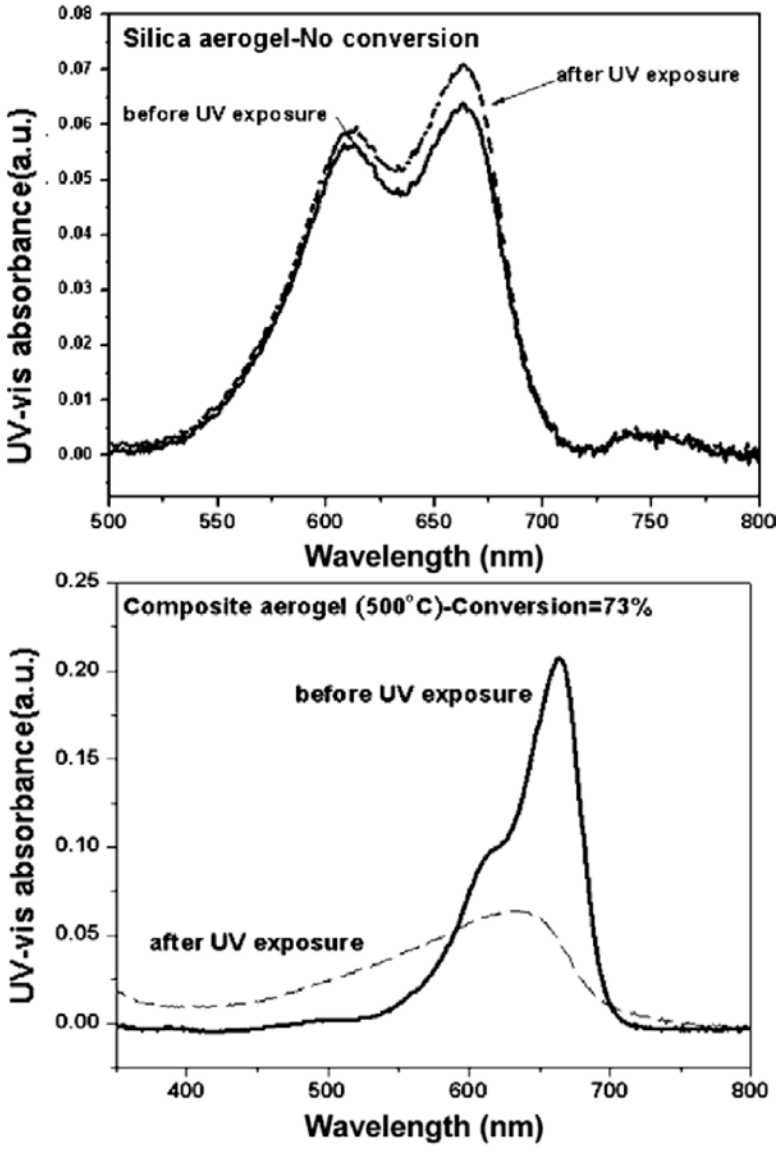

Figure 16.7 Photocatalytic characterization of pure silica and SiO_2–SnO_2 composite aerogels thermally treated at 500°C (reproduced from [30] by permission of Elsevier).

A 2-nm thick ZnO layer was deposited on the inner surface of ultralow density (about 0.5% of full density) nanoporous silica aerogel monoliths [31]. The deposition was performed in a viscous flow reactor using a diethyl zinc/H_2O mixture. Prior to that, a nucleation layer of amorphous Al_2O_3 was deposited in order to prepare a densely hydroxylated surface to minimize any nucleation delays. The coating produced a decrease in surface area and porosity and a corresponding increase in the apparent density. However, the coated aerogel still retained a high surface area and ultralow density. TOF-SIMS images illustrated that the coating was uniform for both the ZnO layer and the Al_2O_3 nucleation layer. The orientation and structure of the ZnO layer was illustrated by the *HREM* images, which showed a layer of crystalline ZnO after deposition at relatively low temperatures (177°C).

The preparation of free-standing *mesoporous* TiO_2–SiO_2 aerogels with hierarchical pore structure, which are expected to have applications in photocatalytic degradation of air pollutants, was reported in [32]. The synthesis involved the use of a solution of titanium isopropoxide in ethanol as TiO_2 precursor, with nitric acid as catalyst. The silica precursor solution was prepared in two steps: the first involving the preparation of a clear polymer solution using Pluronic 123, ethanol, water, and nitric acid and the second involving the addition of *TEOS* to the polymer solution. The two precursor solutions were then mixed with varying Ti/Si ratios, and after gelation *sc-CO_2 drying* was performed. One of the samples was also submitted to *sc-HT drying*; finally, aerogels were calcined at 450°C. The preparation method bears similarities with evaporation-induced self-assembly [33], but without carrying out complete solvent evaporation. Instead the solvent was removed from the gel under supercritical conditions. The aerogels before calcination were opaque, in contrast to silica aerogel prepared without the use of P123. Small-angle *XRD* showed the presence of ordered *mesopores*, which were maintained after supercritical drying and calcination. However, after calcination, *XRD* peak intensity decreases and peaks shift toward higher angles, effects that the authors attribute to possible disorder caused by pore shrinkage. The density of the materials was between 0.2 and 0.56 g cm^{-3} depending on the Ti/Si ratio and the supercritical drying conditions, while surface areas varied between 440 and 840 m^2 g^{-1}. Finally, *TEM* indicated that ordered mesostructure was retained in most cases, but samples with higher Ti content showed TiO_2-rich domains.

All examples reported so far refer to nanocomposite aerogels where the dispersed nanoparticles were made of a simple oxide. While multicomponent or mixed oxides nanophases are desirable to obtain multifunctional composites, it becomes more difficult to find general synthetic strategies due to different chemistry requirements.

A relevant example is related to mixed ferrites, of general formula MFe_2O_4, with M being a divalent ion, whose structural and functional properties can be tuned by the appropriate choice of the divalent ion and which find application in a wide range of areas, ranging from magnetism to catalysis.

A strategy which resulted to be successful and quite general for the preparation of nanocrystalline late first row transition elements dispersed in silica aerogel has been proposed based on a co-gelation procedure followed by *sc-HT drying* [34, 35]. A key role in the successful formation of homogeneous multicomponent aerogels is ascribed to the use of a two-step acid–base-catalyzed procedure that uses urea (carbamide, $CO(NH_2)_2$) as the basic catalyst. In fact, the co-gelation procedure adopted to prepare nanocomposite aerogels in most cases is performed under acidic conditions in order to avoid precipitation of metal hydroxides, which leads to the formation of turbid and inhomogeneous gels. These acidic conditions generally give rise to long gelation times if gelation is performed in a closed container or to a significant solvent evaporation before gelation if it is carried out in an open container. The urea-assisted approach has been successful in achieving fast gelation without precipitation of metal hydroxides.

The precursors were *TEOS*, $Fe(NO_3)_3 \cdot 9H_2O$, and the desired metal nitrate, which were pre-hydrolyzed in acidic conditions before addition of a solution of urea. Gelation was performed in a closed container at 40°C, and *sc-HT drying* was performed. Only a minor volume decrease was observed starting from the sol to the gel and to the aerogel, as it can be seen in Figure 16.8 for the specific case of $CoFe_2O_4$–SiO_2. At the same time,

the weight decreased significantly after supercritical drying so that the obtained aerogels possessed very low density (0.07 g cm^{-3}) and were *mesoporous* with surface areas around 350 m^2 g^{-1}, as assessed by N_2 physisorption measurements. *TEM* micrographs showed *macropores* that could not be assessed by physisorption and indicated that nanoparticles were homogeneously dispersed into the highly porous matrix. After supercritical drying, calcination treatment at temperatures between 450 and 900°C was performed, and the surface area was still high until calcination at 900°C, while full densification was only achieved at 1,200°C. *XRD* of aerogel before calcination and after calcination at 450°C showed only faint peaks not easy to ascribe to specific phases. At 750°C, peaks due to cobalt ferrite became apparent and kept growing up to 900°C. The method was successful in preparing aerogels with different loadings of cobalt ferrite, even if the evolution toward the formation of the final nanocomposite was slightly different, being slower at lower loading. The nanoparticles displayed *superparamagnetic behavior* with blocking temperatures increasing both with loading and with calcination temperature, as reported in Figure 16.9 for the aerogel with 5% (w/w) loading of cobalt ferrite [36].

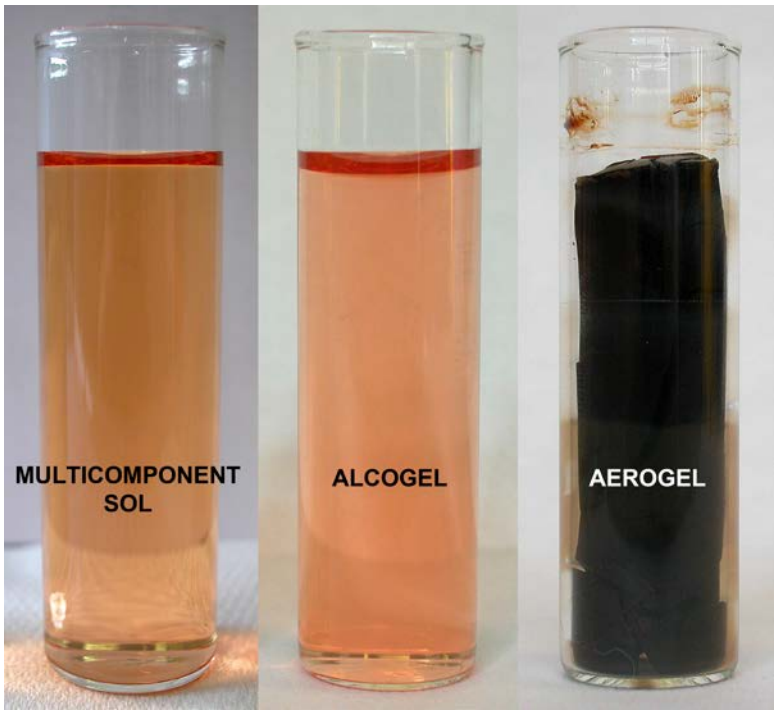

Figure 16.8 Photographs of sol, alcogel, and aerogel for the synthesis of highly porous $CoFe_2O_4$–SiO_2 nanocomposite.

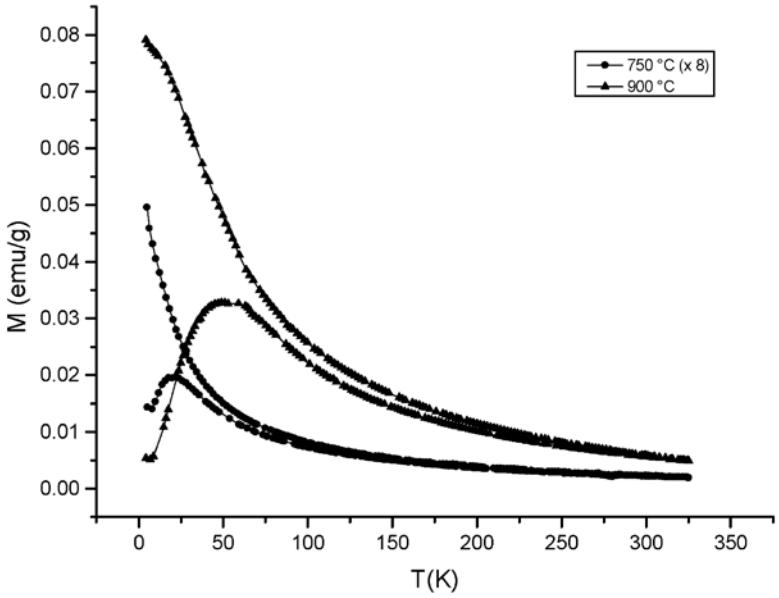

Figure 16.9 ZFC–FC magnetization curves of the $CoFe_2O_4$–SiO_2 nanocomposite aerogel with 5 wt% loading of cobalt ferrite (reproduced from [36] by permission of American Chemical Society).

A more detailed study of the evolution of these aerogels with thermal treatment was carried out with *EXAFS* and *XANES* [37, 38] spectroscopies at both the Fe and Co K-edge, to highlight the nanophases forming at different stages of the synthesis. The evolution was different depending on the loading of $CoFe_2O_4$. At the highest loading (10%, w/w), two separate phases were present after supercritical drying and after calcination at 450°C: Fe was present as six-line ferrihydrite, while cobalt was present in a separate phase, which was later identified as $Co_3Si_2O_5(OH)_4$ [39]. Low loading aerogels (5%, w/w) were calcined at the same temperature and contain Fe and Co in a very disordered environment. After calcination at 750°C, the 5% sample still had two separate phases, while in the 10% sample a significant amount of $CoFe_2O_4$ was already formed. At 900°C, all Co and Fe were present in the form of $CoFe_2O_4$ nanoparticles in both samples with different loadings.

Samples calcined at 450°C were at an intermediate stage toward the formation of the final $CoFe_2O_4$–SiO_2 and $NiFe_2O_4$–SiO_2 nanocomposites and were studied further [39]. To this end, additional aerogels were prepared without using the Fe precursor, i.e. containing only a single Co/Ni intermediate phase. The presence of either Co or Ni silicate hydroxide was clearly evidenced by *EXAFS* and *XANES*, while low-resolution *BF TEM* and high-resolution *BF STEM* images showed evidence that those phases had a layered structure with anisotropic nanostructures. Magnetic measurements further confirmed those findings and evidenced the anisotropic shape effect. It should be pointed out that the observed magnetic behavior was quite similar to the one reported in Co–SiO_2 aerogels [40]. However, in that case the *ZFC–FC* magnetic results were attributed to Co and CoO. The results point out that a detailed structural characterization using selective techniques, such as X-ray absorption spectroscopy, and the comparison with bulk phases is needed.

Falqui et al. [41] further investigated samples consisting of 5 and 10 wt% $CoFe_2O_4$ nanoparticles in the silica aerogel matrix using *HREM*, *STEM* imaging, *EDX*

spectroscopy and *EELS*. For the 10 wt% $CoFe_2O_4$ sample *BF STEM* and *HREM* images showed distinct, rounded $CoFe_2O_4$ nanoparticles, with typical diameters of roughly 8 nm. For the 5 wt% $CoFe_2O_4$ sample, *BF STEM* images and *EDX* measurements showed $CoFe_2O_4$ nanoparticles with diameters of roughly 3 nm. *EDX* measurements indicate that all nanoparticles consist of stoichiometric $CoFe_2O_4$, and *EELS* measurements from lines crossing nanoparticles in the 10 wt% $CoFe_2O_4$ sample show a uniform composition within nanoparticles. *BF STEM* images obtained for the 10 wt% $CoFe_2O_4$ sample showed many "needle-like" nanostructures that typically have a length of 10 nm and a width of 1 nm, and frequently appear to be attached to nanoparticles. These needle-like nanostructures are observed to contain layers with interlayer spacing close to 0.33 nm, which could be consistent with $Co_3Si_2O_5(OH)_4$. This trend was confirmed and studied in detail by Mountjoy et al. [42] that observed the formation of these needle-like structures in $CoFe_2O_4$ and $NiFe_2O_4$-SiO_2 nanocomposites calcined at 450°C and 900°C. In the samples treated at 450°C, high resolution *STEM* images show needle-like nanostructures ~1 nm in width and 10 nm in length. The composition information derived from *EELS* analysis confirms the formation of Co (or Ni) silicate hydroxide phases. After heat treatment at 900°C the needle-like structures have composition similar to ferrite phases (with high Fe content) and they are often found attached to round ferrite nanoparticles. These results reveal a thermal dependent structural evolution of the needle-like nanoparticles from Ni and Co silicate hydroxide phases to ferrite phases that can be explained with an atomic migration and exchange of Si and Fe ions.

The sol–gel procedure involving the use of urea as gelation agent was shown to be very versatile. By using $Ni(NO_3)_2 \cdot 6H_2O$ or $Mn(NO_3)_2 \cdot 6H_2O$ instead of $Co(NO_3)_2 \cdot 6H_2O$, nanocomposite aerogels with loading of 10 wt% of either $NiFe_2O_4$ or $MnFe_2O_4$ nanoparticles dispersed in the highly porous silica matrix were obtained [35]. The evolution of the sample was found to be similar to that observed in the $CoFe_2O_4$–SiO_2 nanocomposites, as it can be inferred from Figure 16.10 reporting the *XRD* patterns at different calcination temperatures. As also confirmed by a detailed *EXAFS* and *XANES* study on the formation of $NiFe_2O_4$–SiO_2 [43] and $MnFe_2O_4$–SiO_2 [44] highly porous nanocomposites, after supercritical drying and calcination at 450°C two separate phases are present, one containing Fe and one containing either Ni or Mn. At 750°C, the ferrite phase began to form and the formation was completed either by prolonging the treatment at 750°C or by a shorter calcination at 900°C.

The two step urea-assisted co-gelation procedure was also successfully extended to $ZnFe_2O_4$-SiO_2 as well as $CuFe_2O_4$-SiO_2 aerogels [45, 46], see Figure 16.10. Overall, it was found that only slight adjustments, mainly based on the thermal processing conditions of the aerogels, had to be adopted to obtain the optimal ferrite/silica composite depending on the chemical composition. A somehow similar result was obtained in the study of a uniform route for unsupported MFe_2O_4 (M = Co, Ni, Cu, Zn) bulk aerogels by an epoxide addition route followed by *sc-LT* drying [47].

Loche et al. [48] proposed to extend the two step urea-assisted co-gelation procedure to other spinel nanoparticles supported on silica aerogel, such as nickel cobaltite. These nanocomposites were obtained in the form of low density aerogels containing $NiCo_2O_4$ nanoparticles of 4 nm. In this case the direct oxidation at 900°C gives rise to two separate Ni and Co phases (Ni_2SiO_4 and CoO), whereas a reduction step followed by a thermal

treatment at 450°C allow to obtain a pure $NiCo_2O_4$ phase, see Figure 16.10, as also confirmed by *EXAFS* and *XANES*.

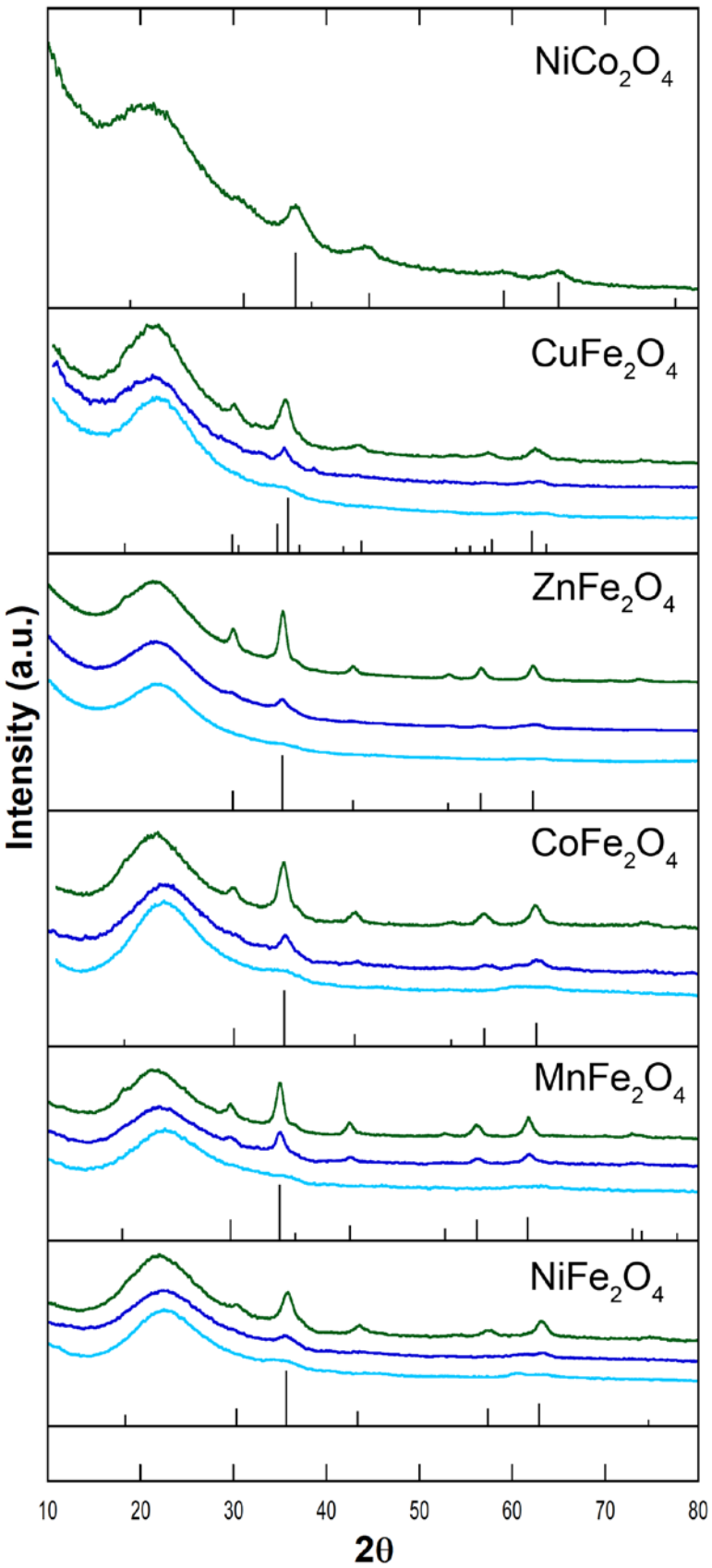
NiCo2O4
CuFe2O4
ZnFe2O4
CoFe2O4
MnFe2O4
NiFe2O4
Intensity (a.u.)
10
20
30
40
50
60
70
80
2θ

Figure 16.10 XRD patterns of a series of 10 wt% MFe_2O_4–SiO_2nanocomposites submitted to different calcination treatments: light blue (450°C), blue (750°C) and red (900°C). The $NiCo_2O_4$ sample is prepared with a reduction step followed by calcination at 450°C. Black bars represent the reference patterns.

It is important to point out that due to their high purity and crystallinity, mixed metal ferrites dispersed on silica aerogels represent ideal systems to address important structural and microstructural aspects on the structure of spinels, such as the inversion degree and its size- and composition-dependency, which has been studied in detail by *EXAFS* and *XANES*, by total X-ray Scattering and by Mössbauer spectroscopy.

In fact, *EXAFS* and *XANES* proved to be extremely powerful in order to study the degree of inversion in the MFe_2O_4 (M = Mn, Co, Ni, Zn, Cu) spinel nanoparticles [49, 50, 46]. In particular, the degree of inversion in nanosized MFe_2O_4 (M = Mn, Co, Ni) was found to be quite close to the values generally observed in the corresponding bulk ferrites, with $MnFe_2O_4$ nanoparticles presenting the lowest degree of inversion (0.20), followed by $CoFe_2O_4$ nanoparticles (0.68), and $NiFe_2O_4$ (1.00).

Carta et al. [50] carried out an *EXAFS* and *XANES* study of zinc ferrite nanocrystals dispersed in a highly porous silica aerogel matrix calcined at different temperatures. The results indicate that the inversion degree of the zinc ferrite spinel structures varies with particle size increasing from 0.21 for 11 nm nanoparticles (obtained by treating the nanocomposite at 900°C) to 0.41 for 4 nm nanoparticles (750°C). This confirms that the role of the silica matrix is limited to keep the nanoparticles far apart and that the degree of inversion is an intrinsic characteristic of ferrite structures and it is not influenced by the presence of the matrix. The same research group [51] has explored the use of total X-ray scattering method as complementary technique for the study of $MnFe_2O_4$-SiO_2 aerogel nanocomposites, determining a pair distribution difference curve obtained by subtracting the total pair distribution function of the matrix from that of the nanocomposite, allowing one to selectively study the structural environment of the nanoparticles, with an approach that should be considered as complementary to *EXAFS* but is also sensitive to the middle range order.

Recently, *EXAFS* and *XANES* techniques have been used to demonstrate the presence of a cubic iron sub-lattice in tetragonal $CuFe_2O_4$ nanoparticles (6-7 nm) dispersed in aerogel matrix [46]. The results demonstrate that the Cu^{2+} ions located in octahedral sites undergo a Jahn-Teller distortion that does not have influence on the coordination of the Fe^{3+} ions giving rise to two sub-lattices: one tetragonal and one cubic for Cu^{2+} and Fe^{3+} ions respectively.

EXAFS and *XANES* [48] have also been very useful in comparing nanophase nickel cobaltite dispersed in silica aerogel with an unsupported nickel cobaltite sample. This study pointed out for the first time that the unsupported sample has a Ni:Co molar ratio higher than the nominal ratio of 1:2 and a larger than expected average overall oxidation state of the cobalt and nickel cations. This is achieved retaining the spinel structure, which accommodates vacancies to counterbalance the variation in oxidation state.

Casula et al. [52] also used Mössbauer Spectroscopy to investigate magnetic nanosized ferrites MFe_2O_4 (M = Mn, Co, Ni) dispersed in silica aerogels to gain insights on the superparamagnetic relaxation and on the inversion degree. Magnetic ordering at room temperature varies from superparamagnetic in the $NiFe_2O4$ sample, highly blocked (~70%) in the $MnFe_2O_4$ sample and nearly fully blocked in the $CoFe_2O_4$ sample. A fitting procedure of the Mössbauer data has been used in order to resolve the spectrum into the tetrahedral and octahedral components; in this way, an inversion degree of 0.68

(very close to bulk values) was obtained for 6 nm silica-supported $CoFe_2O_4$ nanocrystals. Ferrite nanoparticles dispersed in a silica aerogel have been exploited as catalysts for the production of *MWCNTs* by *CCVD*.

Loche et al. [53] employed highly porous aerogel nanocomposites containing three different ferrite nanoparticles (Co, Mn and Ni ferrites). The authors observed a different catalytic behavior of the three ferrite-silica aerogels that is attributed to a different reducibility in the *CNTs* synthesis environment. The higher catalytic activity of the $NiFe_2O_4$ nanoparticles is due to the formation of NiFe alloy (the phase promoting the *MWCNTs* growth) during the *CCVD* process. The $NiFe_2O_4$-SiO_2 catalyst gives rise to high yields of good quality carbon nanotubes with deposition temperatures in the range 500-650°C.

16.2.2 Non-silica aerogels containing oxide nanoparticles

While almost all papers on nanocomposite aerogels containing metal oxide nanoparticles dispersed in an insulating matrix refer to silica-based systems, a few examples are also available for other matrices.

CuO/*RF* samples were prepared using a $CuCl_2 \cdot xH_2O$/epichlorohydrin sol to catalyze cogelation of the system (Chap. Phenolic-type Aerogels and Derived Carbons: The Paradigms of Resorcinol-Formaldehyde and Polybenzoxazine Chemistries), using *DMF* as common solvent [54]. Drying was performed by *sc-*CO_2. The copper oxide remained trapped in the *mesoporous* voids of the *RF* network. Samples were *mesoporous* and did not present any crystallinity. After pyrolysis at 400°C, the dominant crystalline phase was cubic metallic Cu, probably by direct oxidation of *RF* by CuO. Similar smelting reactions were observed in analogous Fe_2O_3/*RF* composites at much higher temperatures [55], at which the *RF* network is first converted to a porous carbon network [56].

16.3 Aerogels Containing Metal and Alloy Nanoparticles

The preparation of nanocomposite aerogels made out of zero-valent metal or alloy nanoparticles in an insulating aerogel matrix has attracted a great deal of effort in view of the preparation of materials for catalysis, biomedicine, optoelectronics, and sensors. As it is the case for all sol–gel nanocomposites, silica is by far the most investigated matrix for supporting metal/alloy nanoparticles, although alumina, titania, chromia, and polymer supports have also been proposed.

On the other hand, a variety of metal nanoparticles have been considered either on the basis of the ease of reducibility, with the aim of developing optimized synthetic protocols, or in order to provide the desired functionality to the nanocomposite. Noble metal nanoparticles are the most investigated as they meet both requisites: they can be easily obtained and stored in the zero-valent state; they are catalytically active toward a wide range of chemical processes [57–61]; and they can have biomedical applications such as antimicrobial activity [62]. Moreover, metal nanoparticles exhibit characteristic surface plasmon bands and when hosted in dielectric matrices, due to the refractive index mismatch, can give rise to enhanced optical effects, namely, surface enhanced Raman scattering [63].

Transition metals and their alloys have also attracted much attention due to their magnetic properties and due to their potential in catalysis thanks to the occurrence of different oxidation states.

In the following, we will summarize how the issue of the control over the nanocomposite formation has been recently addressed.

16.3.1 Silica-based Aerogels containing metal and alloy nanoparticles

An ideal approach for producing aerogel-supported functional nanophases relies on the deposition of metal nanoparticles on a pre-formed aerogel matrix, as the addition of the dispersed phase can be performed without interfering with the sol–gel process, and non-aggregated metal nanoparticles are intrinsically produced. This approach was first demonstrated by Hunt et al. [64] and by Kucheyev [31] for other nanocomposite materials and has recently been used for the preparation of Ru–SiO_2 nanocomposite aerogels by atomic layer deposition of Ru on a low-density silica aerogel using bis-cyclopentadienyl ruthenium [65]. However, at present this technique can be promising only for metal deposition on very thin layers, as large-scale inhomogeneity was observed. In particular, in correspondence with the cracks in the silica substrate a high concentration of Ru was found. The authors suggest that new metal precursors with higher vapor pressures or new reactors should be designed in order to promote effective diffusion of the metal precursor in matrices with porosities on the nanometer scale and therefore extend the applicability of this approach.

A more general procedure for the preparation of metal–silica aerogel nanocomposites is based on the supercritical drying of a silica alcogel previously soaked in a metal solution.

Aerogels made out of gold supported on silica–chitosan (90:10 ratio) monoliths have been prepared by dipping the alcogels into an ethanolic solution of $HAuCl_4$ and performing *sc-CO_2 drying* [66]. In this way, a monolithic aerogel where Au(III) bridged to the biopolymer–silica support (thanks to the amino and hydroxyl groups present in the chitosan) was obtained, which was then reduced by UV irradiation (Chap. Biopolymer-Containing Aerogels: Chitosan-Silica Hybrid Aerogels). The oxidation state of the metal and the size and size distribution of the gold nanoparticles were studied by photoacoustic spectroscopy. Compared to traditional optical absorption, this method is more sensitive and can be used on both transparent and opaque materials without the need of sample preparation, and therefore it is very suitable for monolithic aerogels. The characterization results suggest that the Au nanoparticles were mainly located on the surface of the matrix; in this respect, the role of the biopolymer-modified silica (compared to pure silica) is not clear as it does not ensure a homogeneous metal distribution by coordinating the Au(III) precursor. As structural and morphological characterization (in particular *TEM*) is missing, it is hard to provide additional evaluation on the validity of this approach, which is in any case limited to the formation of metals obtainable by photolysis-induced reduction (thermal reduction would induce pyrolysis of the polymer-modified matrix).

In an alternative approach, Morley et al. [67, 68] describe a similar procedure, which is effective for the preparation of metal–SiO_2 nanocomposites based on the use of supercritical carbon dioxide for the impregnation of a preformed silica alcogel with a suitable metal complex and for the removal of the free ligand after the reduction step. Pd– and Ag–SiO_2 aerogels, which can be used as active catalysts, were effectively obtained by this procedure where supercritical carbon dioxide was used as a recyclable solvent, which does not alter the porous structure of the matrix. However, in addition to the many

steps required, a major disadvantage of this procedure is that it requires solubility of metal complexes in *sc-CO_2*.

The properties of *sc-CO_2* in the development of novel processes for the synthesis of nanostructured materials were also exploited in the case of Pt–SiO_2 aerogels obtained by impregnation of preformed commercial silica aerogels [69]. By making use of *sc-CO_2* as the solvent for the deposition of the metal precursor (dimethyl cyclooctadiene platinum-II), Pt–SiO_2 nanocomposites with a narrower size distribution compared to the results obtained by Morley et al. [67, 68] were obtained. However, metal nanoparticles seem to be mainly deposited on the outer surface of the silica aerogel (see Figure 16.11). By applying the same deposition procedure on different substrates (carbon black, alumina, silica, and silica aerogel), the authors were able to show that particle formation and growth was mainly governed by the strength of the interaction between the organometallic precursors and the support.

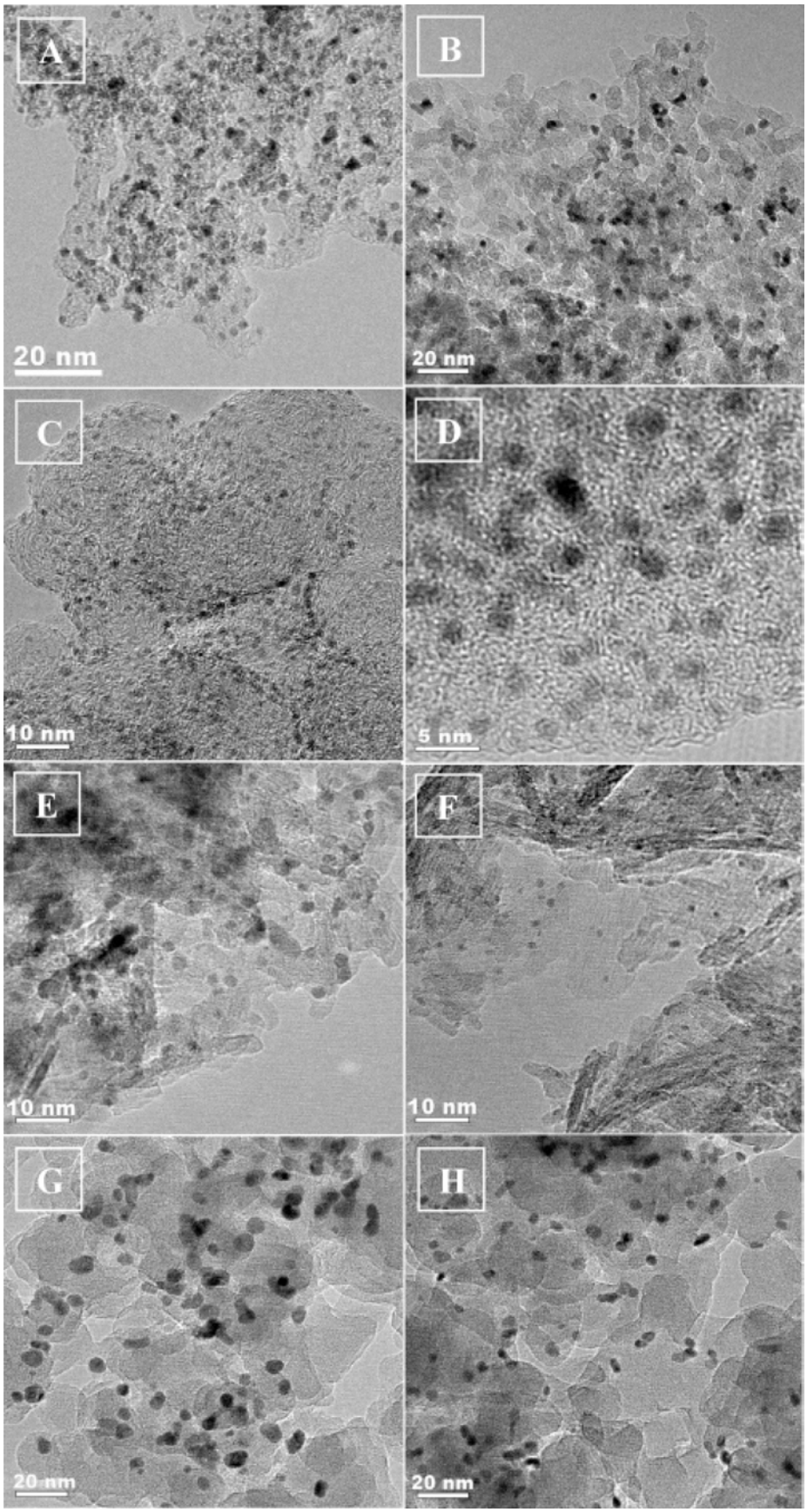
A
20 nm
B
20 nm
C
10 nm
D
5 nm
E
10 nm
F
10 nm
G
20 nm
H
20 nm

Figure 16.11 HRTEM micrographs of supported Ru and Pt nanoparticles on different substrates: **A.** carbon aerogel, **B.** silica aerogel, **C.** carbon black, **D.** Nafion, **E, F.** γ-Al_2O_3, **G, H.** SiO_2 (reproduced from [69] by permission of American Chemical Society).

Impregnation of silica alcogels obtained by an acid/base two-step catalysis by saturated ethanolic solution of Ni(II) and Pd(II) acetylacetonates, followed by *sc-HT drying*, has been used for the preparation of Ni–SiO_2 and Pd–SiO_2 nanocomposites [70]. Metal nanoparticles of about 14 nm were obtained after supercritical drying without the need of further reduction treatment, which was tentatively ascribed to a reducing effect of supercritical ethanol. The synthetic procedure itself is quite straightforward, although time-consuming (sample preparation overall requires over 1 month) and very high surface areas (higher than 800 $m^2\ g^{-1}$) were obtained. A major drawback is in the inhomogeneous distribution of the nanoparticles within the matrix, which the authors found to be responsible for the moderate conversions obtained by using those aerogels as catalysts for *Mizoroki–Heck* C–C coupling reactions. Poor reusability of the catalyst was also observed (due to metal leaching) probably due to the weak interaction or distribution of the metal nanoparticles on the silica surface.

In order to improve the design of Ni–SiO_2 and Pd–SiO_2 aerogel catalysts, a co-gelation route followed by *sc-CO_2 drying* and thermal treatment was used [60]. In that approach, complexation of Pd or Ni(II) acetates in ethanol by organofunctional siloxanes of the type $(CH_3O)_3$–Si–X (where X is a group capable of binding the metal, such as ethylenediamine or diethylenetriamine) was first carried out and then *TEOS* was added and co-gelled. The corresponding aerogel obtained by *sc-CO_2 drying* was then either reduced at 500°C or first calcined and then reduced. Direct reduction of the aerogel may lead to carbon contamination, which in this case can be advantageous since metals on carbon catalysts are known to have enhanced catalytic performance in C–C coupling reactions. Good catalytic results, with conversions as high as 99%, were obtained in particular by the use of the Pd–SiO_2 aerogels, which have 1–2 nm metal nanoparticles well distributed within a *macroporous* silica matrix, with a surface area in the 500–700 $m^2\ g^{-1}$ range. That method, thanks to the use of the complexing organosilane in the sol–gel synthesis, which was first developed for xerogels [71], has been very suitable for the preparation of homogeneous nanocomposites with non-aggregated nanoparticles. A useful further implementation would be the achievement of particle size control in order to tailor the nanoparticle size for selected applications.

The design of Pd–SiO_2 active catalysts for organic reactions, such as hydrogenation of α,β-unsaturated aldehydes and C–C formation by *Heck coupling*, has been also reported [59]. By adapting a method previously proposed for pure silica aerogels [72], Pd–SiO_2 aerogels were obtained by a sol–gel procedure that makes use of an ionic liquid as the solvent, which can be removed by conventional solvent extraction techniques. In particular, a colloidal suspension of palladium nanoparticles having 1 nm size was first obtained by heating at 80°C a dispersion of palladium(II) acetate and triphenylphosphine in an ionic liquid. Once *TEOS* and formic acid were added, gelation took place in 15 min. Aging over a few weeks was required in order to strengthen the gel network, and the aerogel was finally obtained by removing the ionic liquid from the monolith by refluxing acetonitrile overnight. Although it was not possible to discuss the quality of the nanocomposites as no extensive structural investigation was presented, the advantage of

that approach was related to the use of a green solvent, which enables the manufacture of aerogels by more viable and cleaner synthetic routes.

The preparation of nanocomposites by co-gelation of preformed colloidal nanoparticles and of *TEOS* has also been adopted for the preparation of Ag–SiO_2 [73] and Au–SiO_2 [74] nanocomposites.

Smith et al. have prepared Ag–SiO_2 aerogels by adding a silver colloidal suspension obtained by the Creighton procedure [75] to pre-hydrolyzed *TEOS* and then submitting the gel to *sc-CO_2 drying*. Characterization of the aerogels was performed by optical absorption spectroscopy and the data were modeled in order to determine whether nanoparticles were surrounded by air or by the silica matrix. The calculation was based on the shift in the absorption profile, which could be ascribed to the difference in the dielectric contrast of the two environments. It was found that the fraction of Ag surface area in contact with silica was 46%. The proposed method is a promising way to determine the metal accessible area for catalytic application in nanocomposites that do not present aggregation. Unfortunately, those data were not supported by any structural and morphological characterization results.

Balkis Ameen and coworkers have reported a cost-effective preparation of Ag–SiO_2 by co-gelation of *TEOS* and $AgNO_3$ under acid catalysis followed by subcritical drying of the corresponding alcogel [63]. Subcritical drying includes solvent exchange to remove water from the alcogel, aging in *TEOS* solution to improve the network stiffness and strength, again solvent exchange to absolute ethanol, and finally drying at 120°C. The resulting nanocomposite aerogels contained metallic silver, which was probably formed by free radicals of the alcohol generated within the sol system, with particle sizes in the 6–8 nm range. The particle size increased with metal loading, which was varied from 1, 5, and 25% (w/w). Those nanocomposites exhibited a large surface area for moderate loadings (surface area values drop from 850 to 300 $m^2\ g^{-1}$ from pure silica to a 25%, w/w, nanocomposite) and a relatively dense texture. As the metal loading affects the average particle size, the catalytic behavior of these nanocomposites for the selective oxidation of benzene to phenol as a function of metal particle size was also investigated [57]. The highest selectivity was obtained in catalysts containing smaller nanoparticles, whereas an increase of conversion and a decrease of selectivity were observed with increasing Ag particle size.

Au–SiO_2 aerogels with a metal loading from 0.2 to 25% (w/w) were successfully obtained starting from preformed colloidal gold nanoparticles [74]. A silica alcogel obtained by a basic catalysis of *TMOS* was solvent-exchanged (from methanol to toluene) and immersed in a toluene suspension of colloidal Au nanoparticles obtained by the Brust method [76], as shown in Figure 16.12. In order to obtain aerogels, *sc-CO_2 drying* was then performed so that the mild drying conditions did not affect the adsorption of thiol molecules from the Au surface. The advantage of this procedure relies on the assembly of nanocomposites with both known textural features of the matrix and size of the nanoparticles. In particular, by adopting this procedure for colloidal nanoparticles with different sizes, the authors concluded that dipole–dipole-induced interactions were responsible for the adsorption of the highly polarizable Au core on silanols. In fact, larger metal nanoparticles were adsorbed more readily, whereas nanoparticle uptake was slowed down when the silica surface was modified by the addition of hydrophobic $-Si(CH_3)_3$ groups introduced by hexamethyldisilazane.

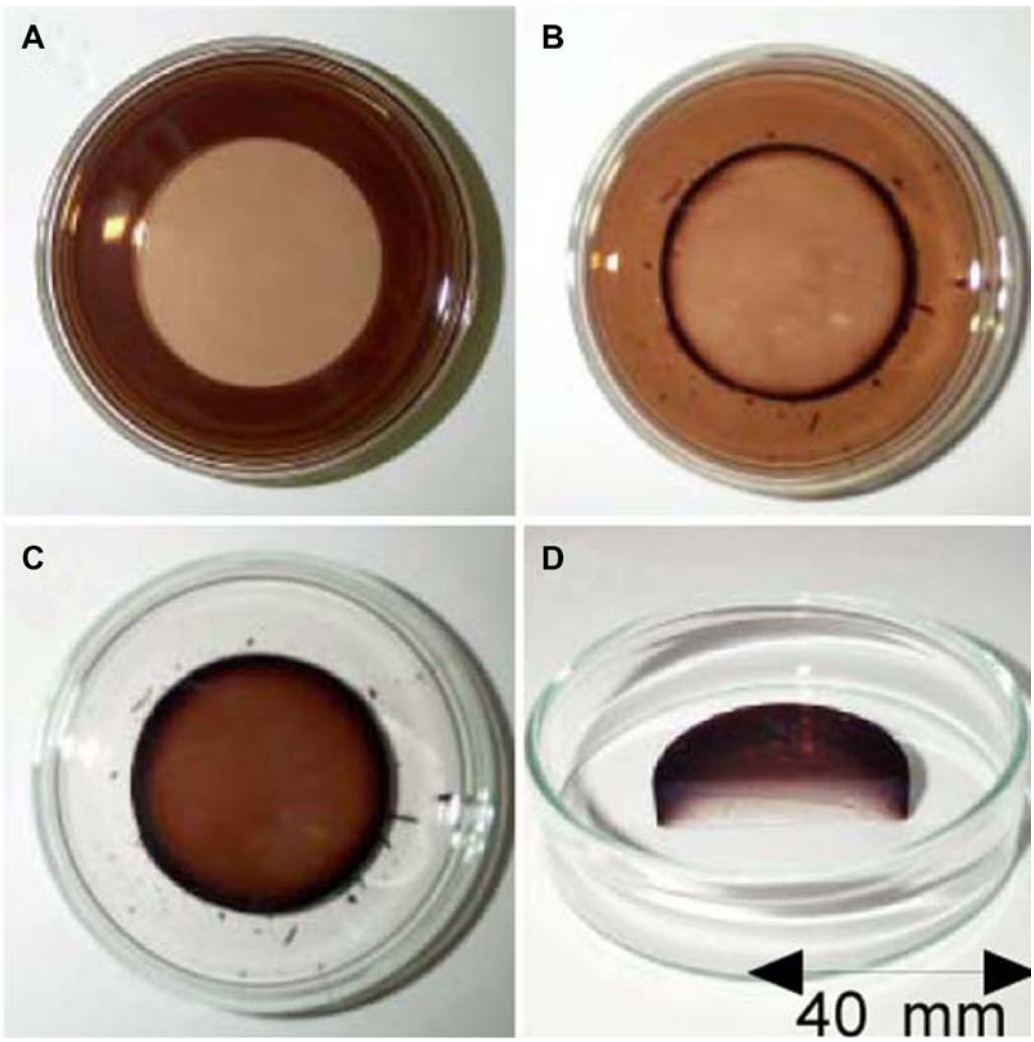

Figure 16.12 Photographs of a silica wet gel immersed in a colloidal suspension of gold nanoparticles at increasing times **A**–**C.** and of the Au–SiO_2 composite aerogel **D.** (reproduced from [74] by permission of Springer).

The same authors optimized the above synthesis for the design of aerogel catalysts by preparing nanocomposites made out of Au nanoparticles supported on titania-coated silica [77]. For that purpose, once the silica alcogel was obtained and solvent exchanged, it was immersed into titanium isopropoxide and then supercritically dried with *sc-CO_2*. The powdered titania-coated aerogel was immersed in a toluene suspension of colloidal Au nanoparticles prepared by the Brust method, the nanoparticle uptake by the aerogel being monitored by the decoloration of the suspension, and finally the impregnated powder was dried by calcination at 400°C. In that case, as opposed to previous results [74], a significant decrease in pore diameter and pore volume was observed upon metal uptake by the porous matrix as a consequence of the impregnation of the aerogel into the liquid: larger pores are more fragile and collapse more easily.

Those materials are promising for the catalytic oxidation of CO, as gold has been reported to be very active as catalyst and TiO_2 is expected to increase the resistance of gold nanoparticles to sintering. The catalytic assays, reported in detail in [58], indicate

that the Au nanoparticles actually grow more slowly with respect to what is observed for other catalysts: after calcination at 700°C, the nanoparticles grow from the original size of 2.6 to about 5 nm. The authors showed that the textural modification induced by impregnation of the aerogel in toluene did not affect the CO conversion and that oxidation activity increased monotonously with metal content. This latter result should indicate that all the Au nanoparticles have the same activity and is therefore ascribed to the good dispersion of the samples. At higher loadings, however, the particle size increased and the reaction rate decreased significantly.

Gold–silica aerogels were also prepared by adding commercial colloidal Au nanoparticles to about-to-gel silica sols prepared under either acid or base catalysis. After gelation, solvent exchange to acetone was performed and finally the aerogels were obtained by *sc-CO_2* [78]. This procedure turned out to be very general in the preparation of silica-based composite aerogels and is based on the use of the about-to-gel silica sol, which acted as a "nano-glue" in the incorporation of nano- and microparticles into the silica network, and provided therefore to the dispersed phase a high stability toward further processing (exposure to solvents, temperature, and pressure) [79]. By that route, the authors were able to include into the silica network preformed colloidal nanoparticles (Au, Pt) as well as carbon black, titania, and zeolite powders. In particular, by selecting the appropriate colloidal precursor, Rolison et al. were able to immobilize polycrystalline Au nanoparticles ranging in size from 5 to 100 nm into the silica aerogel network [78]. Although the gold loading in the nanocomposite was quite low (0.1%, v/v), two main advantages of this procedure were demonstrated. First of all, the addition of the colloidal nanoparticles to the about-to-gel silica colloidal sol allowed effective gluing of the gold nanoparticles to the silica substrate, and no leaching or damage was observed even under repeated washing or during the *sc-CO_2* step. In addition, the potential of those gold–silica composites for sensing or catalytic applications was proven by demonstrating the accessibility of the Au surface by means of direct adsorption of dye species onto the gold surface.

The same authors were able to obtain a biocomposite gel by mixing cytochrome *c* with colloidal gold prior to the addition to the about-to-gel colloidal silica [80, 81]. The heme protein self-assembled on the colloidal Au surface (with a ratio of 10,000 protein molecules per gold nanoparticle) forming assemblies of about 100 nm, which were not altered by insertion into the silica matrix or by *sc-CO_2 drying*. The activity of cytochrome *c* activity was largely preserved, as shown by the visible absorption band due to the metal–ligand coordination of the folded protein known as Soret band, which had an intensity ≥80% of that of the solution protein. It is worth noting that when cytochrome *c*–silica aerogels were prepared, both the protein superstructure and the metal–ligand coordination were damaged, as indicated by the complete disappearance of the Soret band. Indeed, the stabilization of the cytochrome *c* in the aerogel is due to the presence of gold, as specific adsorption of the heme edge onto the gold surface occurs; it is followed by protein self-assembly, which is made possible by the appropriate radius of curvature. Therefore, the authors demonstrated that the design of the appropriate metal–silica nanocomposite aerogel enabled to obtain biocomposite aerogels stable over 6 weeks. The authors applied those biocomposites to gas-phase recognition, as the protein retained its ability to bind nitrogen monoxide. Although the stability of those biocomposites was greatly improved compared to the corresponding xerogels, the response of the

biocomposite varied over the ~6 weeks of performance, as a consequence of further reactivity of the synthesis by-products. Such limit could not be overcome, as purification steps cannot be performed because they would lead to disruption of the protein self-assembly [80].

Magnetic composites were also prepared by adding microparticulate commercial iron to about-to-gel silica colloid; gelation took place in 5–10 min and after solvent exchange to ethanol and finally to acetone; composite aerogels were obtained by *sc-CO_2 drying* [82]. By performing gelation in a superconducting magnet, aerogels with needle-like field-imposed organization of the microparticles were obtained. As expected, the Fe microparticles could not be aligned by applying the magnetic field after gelation. Moreover, when Fe–SiO_2 composite *xerogels* were prepared by gelation in the presence of an external magnetic field followed by slow drying at ambient conditions over 2 weeks, the resulting composites did show aligned magnetic particles but were extremely fragile and brittle. By removing the needle-like arrangement of oriented Fe particles from aged iron–silica aerogels by dissolution of iron, the authors were able to generate a directional macroporosity in the micrometer regime. Selective removal of a magnetically aligned guest phase provides therefore a means to obtain sol–gel materials with extended directional porosity with a range of perspective uses such as scaffolds for biomolecules. The magnetic properties of the Fe–SiO_2 aerogels were not fully interpreted, as the aerogels unexpectedly did not show any residual macroscopic magnetization once the external field was removed. This result was attributed to the random orientation of the magnetic domains in the composite aerogel.

Magnetic nanocomposites have also been prepared by introducing preformed Fe nanoparticles obtained by fast evaporation of iron pentacarbonyl in a *TMOS* methanol-based sol [83]. The Fe–SiO_2 aerogel was obtained by *sc-HT drying* of the alcogel, obtaining a low-density aerogel with pore diameters in the 20–100 nm range. Structural characterization of the original nanoparticles indicated the presence of 15 nm particles with a Fe core and a ~2 nm layer made out of iron oxide (likely magnetite) clusters. Although no *TEM* or *XRD* characterization of the Fe–SiO_2 aerogel was reported, extensive *SQUID* and Mössbauer spectroscopy indicated that the collective magnetic behavior of the interacting pure nanoparticles and of the nanocomposite were similar. Due to the large relative pore size with respect to the nanoparticle size, aggregates of interacting nanoparticles were formed within the matrix; therefore, the method was not successful in isolating the individual magnetic nanoparticles.

It is important to point out that the additional problem of metal oxidation is very common in the preparation of nanocomposites containing non-noble metals. Moreover, as a consequence of lower stability of the zero-valent state, phase separation may be incomplete and interaction with the matrix can occur.

This was also the case in Co–SiO_2 aerogels [40, 84] prepared by *sc-HT drying* of alcogels obtained by co-gelation of *TMOS* and cobalt (II) nitrate under basic catalysis. The supercritical drying conditions promoted the formation of cobalt oxide Co_3O_4, and reduction under a stream of H_2 at 500°C was then performed to promote the formation of metallic Co. Those materials were active toward the Fischer–Tropsch process, exhibiting CO conversions from 5.3 to 19.8% and 22.3% as the metal loading in the catalyst was increased from 2, 6, and 10% (w/w). The relatively low conversion observed in the 10% (w/w) nanocomposite was correlated to its structural properties by a combination of

TEM, *XRD*, and *SQUID*. *XRD* points to the presence of several peaks superimposed on the amorphous silica background, which were attributed to *fcc*-Co, CoO, and $Co_2(Si_2O_5)_2(OH)_2$. The authors were not able to ascribe all phases to the *TEM* data, although needle-like features with ~1 nm diameter were ascribed to metallic Co. Very similar nanostructures have also been observed in silica-based aerogels containing cobalt and nickel, and thanks to extensive structural investigation they have been attributed to metal silicate hydroxides [39].

The preparation of Co-SiO_2 aerogels [85] containing 24 wt% of metallic Co nanoparticles (5 nm) has been also attempted by impregnation of a pre-formed silica matrix with a solution of $Co(NO_3)_2{\cdot}6H_2O$, followed by reduction making use of a borohydride solution followed by freeze drying to obtain the aerogel. The structural and microstructural features of the resulting nanocomposites have not been fully elucidated, and in particular it was not possible to gain information on which cobalt-based nanocrystalline phase is being formed and the porous texture could not be imaged under *TEM*. The novelty of this work, however, was associated to the activity of the aerogels in the catalytic production of H_2 from ammonia borane, a prospective material for hydrogen storage. In particular, it was shown that the aerogel catalyst exhibits 41% higher hydrogen generation rate than the corresponding catalyst supported on an MCM-41 support. The result is ascribed to the small size of the cobalt nanophase and to its finer dispersion within the aerogel matrix, providing therefore more active sites for the formation of transient Co-H bonds, required to promote the conversion of ammonia borane.

Ni/SiO_2 aerogels [86] have been prepared for relevant prospective application such as carbon dioxide capture. It is well known that Ni can have the ability to capture CO_2; however, to overcome the costs of magnetic separation the immobilization into a highly porous matrix is highly desirable. Pre-formed commercial Ni nanoparticles have been deposited on ambient-dried silica aerogel. Although catalytic characterization suffered from disaggregation of the aerogel during tests in water, it was shown that the prepared aerogels are active in the hydration of CO_2, a reaction of interest for carbon dioxide capture.

As a way to stabilize metallic magnetic phases, metal alloys have been prepared. In particular, iron–cobalt alloys have attracted much attention due to their technological relevance to magnetic storage. In the bulk they are soft magnetic materials with saturation induction 15% larger than pure iron and with magnetization values dependent on their composition.

FeCo–SiO_2 aerogels were obtained by *sc-HT drying* of alcogels prepared by co-gelation of *TEOS* and iron and cobalt nitrates under acid catalysis [87, 88]. Formation of the metal phase is obtained by reduction under H_2 flow at temperatures higher than 600°C. The as-obtained aerogels have large surface areas (700–1,000 $m^2\ g^{-1}$) and they are relatively dense as expected for gels obtained under an all-acidic procedure. In particular, by varying the supercritical drying conditions either *microporous* or composite *micro*- and *mesoporous* nanocomposites were obtained, as pointed out by N_2-physisorption measurements. The alloy loading in the nanocomposites was 10% w/w, and the relative iron:cobalt molar ratio was varied from pure Fe to pure Co.

TEM shows that the nanoparticles with diameter ~10 nm were homogeneously distributed within the matrix; *XRD* data indicated that best results were obtained in the

microporous aerogel where after reduction *fcc*-Co and *bcc*-Fe were formed respectively in the composites containing only one metal. In the FeCo–SiO_2 nanocomposites a *bcc* phase expected for the FeCo alloy was detected by *XRD*, and the main peak shifted according to the expected variation of the cell parameter for the FeCo alloy.

As the *XRD* patterns of FeCo and of Fe were quite similar, definitive assessment of the formation of the alloy was achieved by taking advantage of the selectivity of X-ray absorption spectroscopy in studying independently the Fe and Co environment during the nanocomposite formation [89, 90]. *EXAFS* results show that both Fe and Co are in a *bcc* environment, corroborating therefore that the FeCo alloy is actually formed; moreover, it points out that there is no interaction between the nanoparticles and the matrix. The *EXAFS* investigation of the aerogels prior to the reduction treatment also showed that iron and cobalt were initially present in two separate nanocrystalline phases, Co_3O_4 and ferryhidrite, suggesting that the alloy was formed upon an interdiffusion process.

In order to obtain highly porous FeCo–SiO_2 aerogels, we have made use of a urea-assisted co-gelation procedure previously developed for multicomponent oxide nanocomposites [34]. By this route, very low-density nanocomposites with tunable alloy loading and composition were successfully obtained [91], as shown in Figure 16.13. Extensive structural investigation by *EXAFS*, *HREM*, *EDX*, *EELS* has been used to provide compositional information at the nanometer scale for these nanocomposites [92, 93], showing that the nanoparticles were individual *bcc* nanocrystals, that the alloy composition at the nanoscale was very close to the nominal values (see Figures. 16.14 and 16.15), and that the distribution of Fe and Co from *EELS* analysis profiles of nanoparticles was homogeneous with no evidence of oxides within the limit of detection (i.e., 0.2 nm).

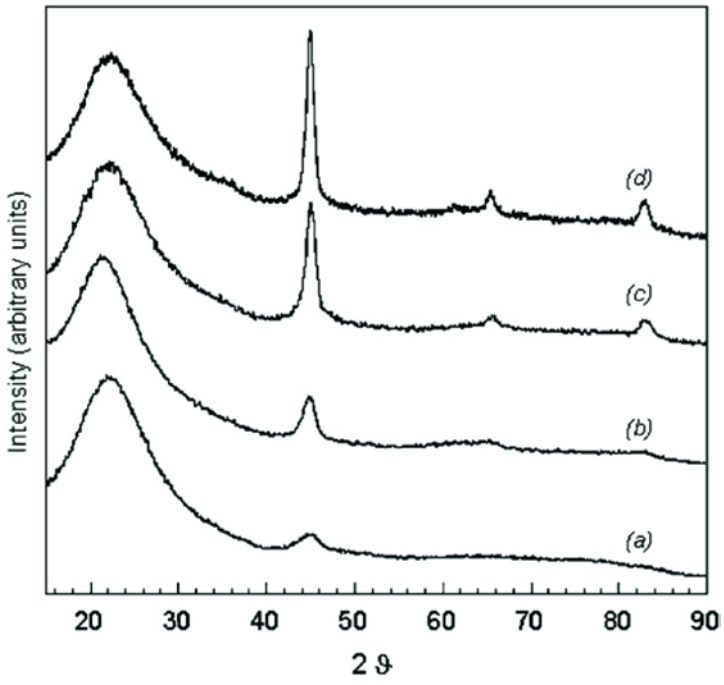

Figure 16.13 XRD patterns of FeCo–SiO_2 nanocomposites with different FeCo loadings: **A.** 3% (w/w), **B.** 5% (w/w), **C.** 8% (w/w), **D.** 10% (w/w) (reproduced from [91] by permission of The Royal Society of Chemistry).

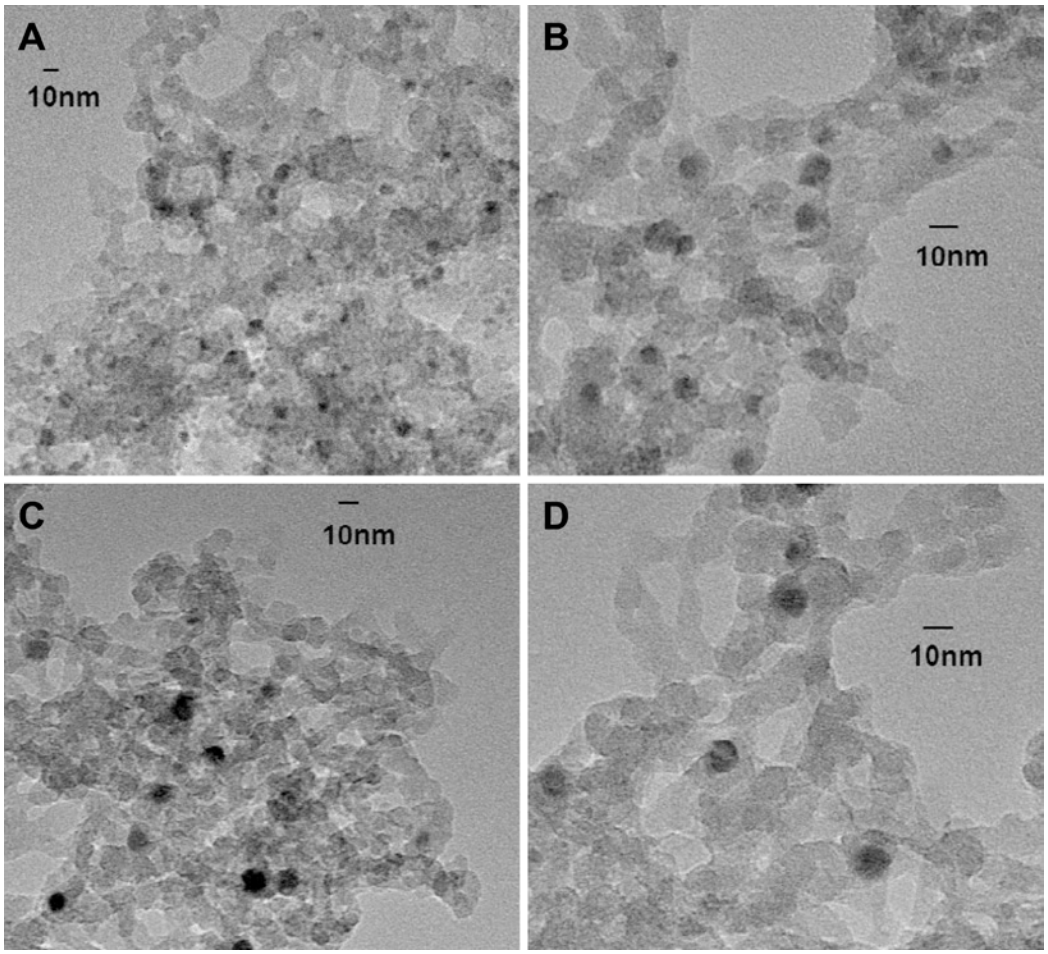

Figure 16.14 BF STEM images of FeCo–SiO_2 nanocomposites with Fe/Co ratio equal to 1 **A**, **B.** and 2 **C**, **D.** (reproduced from [93] by permission of Cambridge University Press).

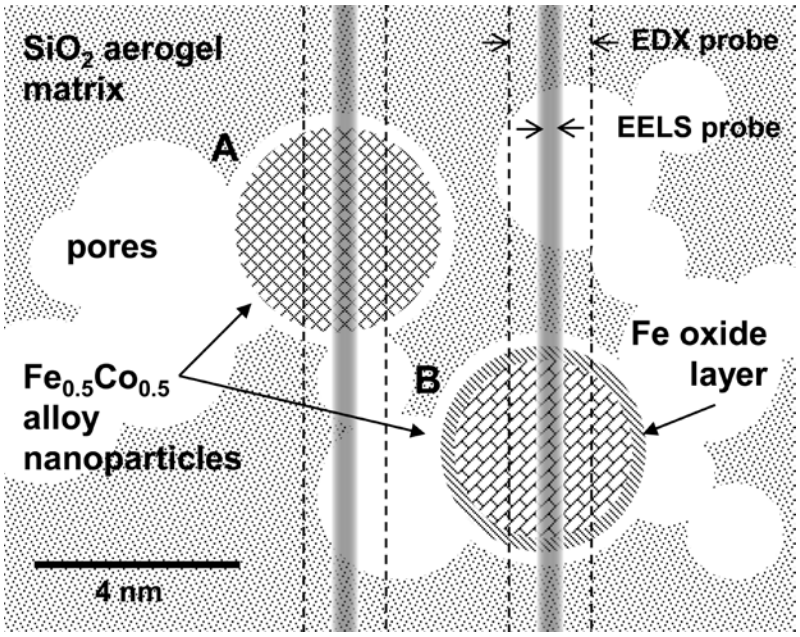

Figure 16.15 Possible scenarios for the microstructure of a 4 nm diameter FeCo alloy nanoparticle: (**A**) nanoparticle consists of a single homogenous alloy phase; (**B**) nanoparticle is covered with a 0.2 nm layer of iron oxide determining a slightly reduced concentration of Fe in the core of the alloy (reproduced from [93] by permission of Cambridge University Press).

It is important to point out that the role of the silica matrix was not limited to the stabilization and isolation of the alloy nanoparticles. In fact, the collective properties of those functional nanocomposites could be tuned as a function of the concentration of the magnetic phase, as well as the relative distance between the nanoparticles, which in turn determined the kind of interaction that will be present. We have demonstrated this idea by extensive magnetic characterization of relatively dense or highly porous FeCo–SiO_2 nanocomposite aerogels prepared either by the acidic or urea-assisted procedure [91]. The comparison showed that nanocomposites having the same alloy loading, the same alloy composition and similar nanoparticle size but different matrix porosities had very different magnetic behavior. The denser aerogel had a larger blocking temperature, which could be ascribed to the occurrence of stronger interactions related to the closer distance between magnetic centers. Those results are an example of the importance of porosity in the design of magnetic nanocomposites, where interparticle interaction is mediated by the matrix.

The characteristics of the highly porous FeCo-SiO_2 aerogel nanocomposites prepared by the urea-assisted method have been exploited in catalytic applications of important heterogeneous gas-phase reactions. The possibility to modify loading and size of FeCo nanoparticles combined with the high porosity and surface area of the aerogel matrix have allowed the authors to study the catalytic effect on the production of *MWCNTs* [94, 95] and on an oil industry-related process such as the low temperature Fischer-Tropsch (FT) reaction [96].

Falqui et al. have modulated the size of the FeCo nanoparticles in order to tune the diameter and the number of walls of the *MWCNTs* synthetized. Interestingly, as the FeCo catalytic nanocrystals remain embedded within the *CNTs*, by dissolving the silica aerogel matrix, magnetic multi-wall *CNT*/FeCo nanocomposites were obtained and investigated by advanced electron microscopy techniques and *SQUID* magnetometry. The *CNT*/FeCo nanocomposites are superparamagnetic with blocking temperatures higher than those expected based on the features of the magnetic alloy core alone, and exhibit magnetic interactions which are mediated by the insulating and shielding effect of the *CNTs*.

In the work of Vanyorek et al. [95] the versatility of sol-gel in the design of tailored composites was applied to the optimization of FeCo–SiO_2 aerogels for *CNT* production by *CCVD* from ethene by the statistical design of experiments approach (Figure 16.16). 19 different aerogels were prepared with variable metal loading on silica, metal composition (Fe:Co ratio), and degree of metal doping (with Ni), as indicated by the statistical design of experiments predictions. *CCVD* experiments with the 19 catalysts in a total of 49 reactions (as opposed to the 27 catalysts and 729 reactions required by a conventional trial-and-error approach) demonstrated that optimal catalysts for *CNTs* growth should contain equimolar amounts of Fe and Co, no nickel doping, and a relatively high loading of alloy in the composite (around 10 wt%).

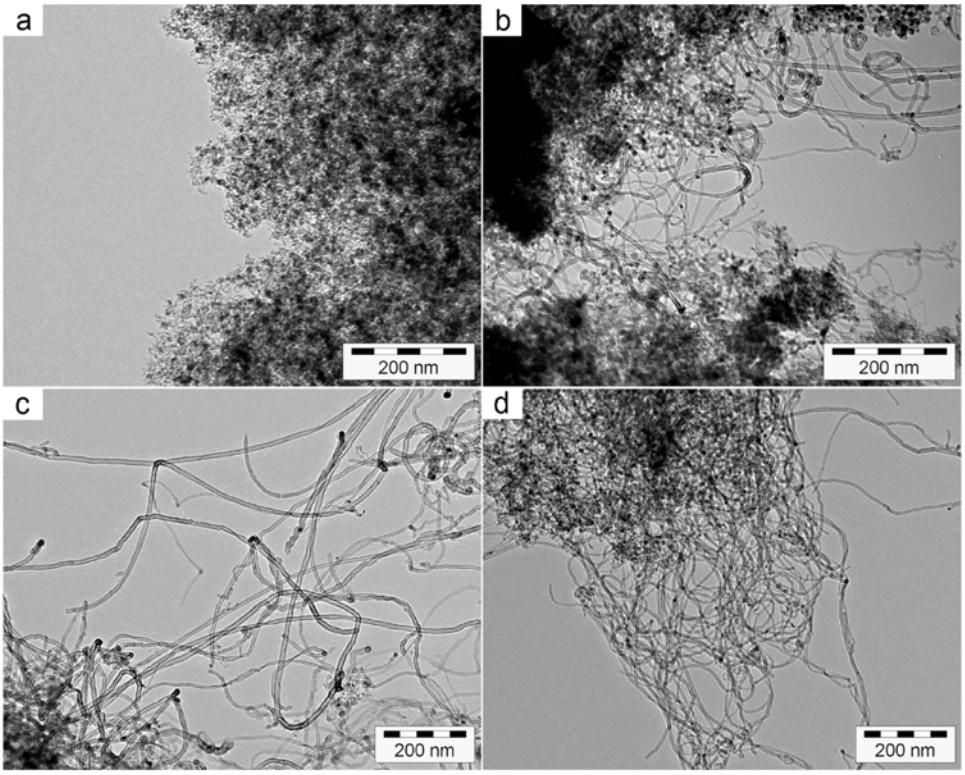

Figure 16.16 TEM images of MWCNTs with increase quality (from **a** to **d**) produced with FeCo-SiO_2 aerogel nanocomposite catalysts (reproduced from [95] by permission of American Chemical Society).

Thanks to the high flexibility of this method, Marras et al. [97] extended the *CNTs* production application of these nanocomposites to embedding Fe and Mo metallic phases in the silica aerogel matrix. The problem of the low solubility in the sol-gel reaction environment of the two Mo precursors employed (ammonium molybdate, $(NH_4)_6Mo_7O_{24}$, and molybdenum(VI) oxide, MoO_3) has been dealt with the use of two additives as potential complexing agents: *DMF* and ethylenediaminetetraacetic acid (EDTA). Despite the *XRD* patterns reveal that a FeMo alloy has never been obtained, homogeneous aerogel nanocomposites containing Fe and Mo nanocrystals (with size of 4–10 and 15 nm, respectively) with a variable Fe:Mo weight ratio have been synthesised after a reduction treatment under H_2 flow at 800°C. The catalytic results show interesting *MWCNT* uptake values around 400 % at 800°C.

Another example on the potential of supported metal alloys for the design of tailored functional materials is provided by Hund et al., who describe a procedure for the preparation of AgAu–SiO_2 nanocomposite aerogels [98]. A silica aquogel prepared from *TEOS* under basic catalysis after repeated solvent exchange was soaked into a solution of $AgNO_3$ and $KAuCl_4$ and then reduced by the addition of formaldehyde under basic conditions. Monolithic aerogels with pore diameters around 7 nm and typical surface areas of 700 $m^2\ g^{-1}$ were obtained by drying under *sc-CO_2* and both *TEM* and spectroscopic investigation confirmed alloying. The authors, however, pointed out the difficulty in obtaining homogeneously loaded gels, and identified kinetic control of the chemical reduction as the key step. Formaldehyde was found to be a suitable reducing

agent since its oxidation rate can be adjusted by the addition of alkali, but the size and size distribution control achieved by this room temperature chemical reduction route was poor with respect to other methods. It is noteworthy, however, that by preparing alloys with different molar ratios the optical properties could be tuned, observing the expected shift of the surface plasmon to lower energies as the Au concentration was increased.

16.3.2 Non-Silica Aerogels containing metal and alloy nanoparticles

Alumina has also been proposed as a suitable matrix for the preparation of functional nanocomposite aerogels. FeCo–Al_2O_3 aerogels were obtained by co-gelation of iron and cobalt nitrates and aluminum tri-*sec*-butoxide in ethanol, followed by *sc-HT drying* and reduction under H_2 flow at 700–800°C [99, 100]. The preparation procedure is fast and leads to the formation of highly porous aerogels (density 0.03 $g\,cm^{-3}$) which after reduction exhibit surface areas around 300 $m^2\ g^{-1}$ and *mesopores* with a diameter in the 20–40 nm range. The overall alloy loading in the nanocomposite is 10% (w/w) and the alloy composition is equimolar.

The structural evolution of the nanocomposites upon thermal treatment is very interesting, as formation of the alloy takes place concurrently with crystallization and phase transition of the alumina matrix. Pure Al_2O_3 aerogels obtained by this procedure exhibited a layered pseudo-boehmite structure (in particular, the ethyl derivative of boehmite was formed as a consequence of esterification during supercritical drying), which upon thermal treatment was converted to nanocrystalline γ-Al_2O_3, and finally at 1,000°C, the thermodynamically stable polymorph α-Al_2O_3 started to crystallize.

Aerogels containing both metals exhibited a similar evolution with temperature; however, the boehmite phase formed at low temperatures was more disordered and upon thermal treatment *XRD* showed peaks at the same positions as γ-Al_2O_3, but with different intensity ratios, suggesting that a phase similar to γ-Al_2O_3 was formed with metal ions partially filling the vacancies. By performing the reduction at 700°C or higher, FeCo alloy nanocrystals that dispersed into γ-Al_2O_3 were successfully obtained. A detailed study of the oxidation state and structure of intermediate phases was performed by *EXAFS*, *XANES* [101], and Mössbauer spectroscopy [102]. Results indicated that after reduction treatment most of the metals were in the zero-valent state with a *bcc* environment, whereas some Co(II) and Fe(II, III) were present and located in the tetrahedral vacancies of the γ-Al_2O_3 structure. Those results were not surprising taking into account that γ-Al_2O_3 has a cation-deficient spinel structure, which can easily accommodate metal ions. *SQUID* investigation showed that the FeCo alloy nanoparticles had a superparamagnetic behavior. The magnetic behavior of the nanoparticles could be varied by changing the temperature and the time of the thermal treatment, which affected the average size, the amount, and relative distance of the magnetic nanocrystals.

Chromia has also been used as a support for noble metals in view of catalytic applications, thanks to its rich oxidation chemistry that makes it very suitable for the catalytic reduction of volatile organic pollutants. Pt– and Au–chromia aerogels with a loading of 0.5 and 0.3% (w/w), respectively, were obtained by incipient wetness impregnation of chromia aerogels with H_2PtCl_6 or $HAuCl_4$ and reduction at 250°C [61]. The chromia aerogel, obtained by *sc-HT drying* of wet gels produced by urea-assisted gelation of chromium nitrate, consisted of 1.5–2 nm CrOOH primary particles giving rise to a highly porous network. It is worth noting that those aerogels had a larger surface area

(610 m^2 g^{-1}), wider pore diameter distribution (average diameter 24 nm), and larger pore volumes with respect to the corresponding aerogel obtained by *sc-CO_2 drying*. The nanocomposite aerogels had surface areas lower than 500 m^2 g^{-1} and displayed an increased activity of the chromia support (which was converted to CrO_2 during the catalytic test) toward oxidations by a factor of 1.25–2.7. Pt-based nanocomposites were also prepared by impregnation of chromia aerogels doped by ceria (10%, w/w): the resulting composite aerogels had surface areas ~400 m^2 g^{-1} and displayed enhanced catalytic performance thanks to the additional effect of Ce, which improved the redox efficiency of the Cr-aerogels by increasing the concentration of oxygen vacancies. The results were interpreted in terms of the textural and surface properties of the different catalysts, rather than in terms of structural/microstructural differences.

As an alternative to inorganic matrices, the use of cellulose has been suggested by Cai et al. as support for silver, gold, and platinum nanoparticles [62]. The nanocomposite aerogels were prepared by *sc-CO_2 drying* of ethanol-exchanged hydrogels obtained by co-gelation of the metal precursors and polysaccharides. The glycol groups of the polysaccharides also acted as reducing agents for the metal. In the case of Au and Pt, however, the use of $NaBH_4$ was required to achieve full chemical reduction. By this procedure, low-cost antimicrobial nanocomposites have been obtained with surface areas up to 400 m^2 g^{-1}, which nevertheless had limited processing thermal and chemical stability compared to silica-based aerogels but higher mechanical strength.

16.4 Concluding Remarks

Considerable improvement has been achieved in the design of functional nanocomposites based on aerogel dielectric matrices, in terms of range of accessible compositions, control over nanoparticle size, distribution and loading, and tailored porous texture.

Since every preparation route has specific advantages and drawbacks, it is not possible to define a general strategy for obtaining nanocomposite aerogels. Nevertheless, metal and metal oxide nanoparticles supported on aerogel matrices with given compositional and microstructural features have been effectively prepared.

The flexibility of the sol–gel route in the chemical design of materials opens up possibilities for new applications for aerogels in very diverse fields ranging from thermal and acoustic insulation to catalysis to magnetism.

Acknowledgments

The authors are very grateful to F. Caddeo, A. Falqui, D. Carta, G. Navarra, and G. Mountjoy for discussion and proof reading.

References

1. I. Ko: Aerogels. In: *Encyclopedia of Chemical Technology*, ed. by Kirk-Othmer (John Wiley & Sons, 1998) pp. 1–3
2. N. Husing, U. Schubert: Aerogels-Airy Materials: Chemistry, Structure, and Properties, Angew. Chem. Int. Ed. **37** 22–45 (1998)
3. G. Piccaluga, A. Corrias, G. Ennas, A. Musinu: Sol-Gel Preparation and Characterization of Metal-Silica and Metal Oxide-Silica Nanocomposites, Mater. Res. Found. **13** 1–56 (2000)
4. T.F. Baumann, J.H. Satcher Jr: Homogeneous Incorporation of Metal Nanoparticles into Ordered Macroporous Carbons, Chem. Mater. **15** 3745–3747 (2003)

5. T.F. Baumann, G.A. Fox, J.H. Satcher Jr, N. Yoshizawa, R. Fu, M.S. Dresselhaus: Synthesis and Characterization of Copper-Doped Carbon Aerogels, Langmuir **18** 7073–7076 (2002)
6. L.I. Casas, A. Roig, E. Rodriguez, E. Molins, J. Tejada, J. Sort: Silica aerogel-iron oxide nanocomposites: structural and magnetic properties, J. Non-Cryst. Solids **285** 37–43 (2001)
7. P. Mendoza Zélis, M.B. Fernández van Raap, L.M. Socolovsky, A.G. Leyva, F.H. Sánchez: Magnetic Hydrophobic Nanocomposites: Silica Aerogel/Maghemite, Physica B **407** 3113–3116 (2012)
8. M.F. Casula, A. Corrias, G. Paschina: Iron oxide-silica aerogel and aerogel nanocomposite materials, J. Non-Cryst. Solids **293–295** 25–31 (2001)
9. C. Cannas, M.F. Casula, G. Concas, A. Corrias, D. Gatteschi, A. Falqui, A. Musinu, C. Sangregorio, G. Spano: Magnetic Properties of γ-Fe_2O_3-SiO_2 Aerogel and Xerogel Nanocomposite Materials, J. Mater. Chem. **11** 3180–3187 (2001)
10. F. Del Monte, M.P. Morales, D. Levy, A. Fernandez, M. Ocana, A. Roig, E. Molins, K. O'Grady, C.J. Serna: Formation of γ-Fe_2O_3 isolated nanoparticles in a silica matrix, Langmuir **13** 3627–3634 (1997)
11. L.I. Casas, A. Roig, E. Molins, J.M. Greneche, J. Asenjo, J. Tejada: Iron oxide nanoparticles hosted in silica aerogels, Appl. Phys. A **74** 591–597 (2002)
12. M.B.F. van Raap, F.H. Sanchez, C.E.R. Torres, L. Casas, A. Roig, E. Molins: Detailed magnetic dynamic behaviour of nanocomposite iron oxide aerogels, J. Phys. Condens. Matter. **17** 6519–6531 (2005)
13. M. Popovici, M. Gich, A. Roig, L. Casas, E. Molins, C. Savii, D. Becherescu, J. Sort, S. Surinach, J.S. Munoz, M.D. Baro, J. Nogues: Ultraporous single phase iron oxide-silica nanostructured aerogels from ferrous precursors, Langmuir **20** 1425–1429 (2004)
14. A. Lancok, K. Zaveta, M. Popovici, C. Savii, M. Gich, A. Roig, E. Molins, K. Barcova: Mössbauer studies on ultraporous Fe-Oxide/SiO_2 aerogel, Hyperfine Interact. **165** 203–208 (2005)
15. M.B.F. van Raap, F.H. Sanchez, A.G. Leyva, M.L. Japas, E. Cabanillas, H. Troiani: Synthesis and magnetic properties of iron oxide-silica aerogel nanocomposites, Physica B **398** 229–234 (2007)
16. P. Fabrizioli, T. Burgi, M. Burgener, S. van Doorslaer, A. Baiker: Synthesis, structural and chemical properties of iron oxide-silica aerogels, J. Mater. Chem. **12** 619–630 (2002)
17. H. Maleki, L. Durães, B.F.O. Costa, R.F. Santos, A. Portugal: Design of multifunctional magnetic hybrid silica aerogels with improved properties, Microporous Mesoporous Mater. **232** 227-237 (2016)
18. H. Maleki, L. Durães, A. Portugal: Development of Mechanically Strong Ambient Pressure Dried Silica Aerogels with Optimized Properties, J. Phys. Chem. C **119** 7689−7703 (2015)
19. B.J. Clapsaddle, A.E. Gash, J.H. Satcher, R.L Simpson: Silicon oxide in an iron(III) oxide matrix: the sol-gel synthesis and characterization of Fe-Si mixed oxide nanocomposites that contain iron oxide as the major phase, J. Non-Cryst. Solids **331** 190–201 (2003)
20. A.E. Gash, T.M. Tillotson, J.H. Satcher Jr, J.F. Poco, L.W. Hrubesh, R.L. Simpson: Use of epoxides in the sol-gel synthesis of porous iron(III) oxide monoliths from Fe(III) salts, Chem. Mater. **13** 999–1007 (2001)
21. C.-T. Wang, S.-H. Ro: Nanocluster iron oxide-silica aerogel catalysts for methanol partial oxidation, Appl. Catal. A: General **285** 196–204 (2005)
22. M.F. Casula, A. Corrias, G. Paschina: Nickel oxide-silica and nickel-silica aerogel and aerogel nanocomposite materials, J. Mater. Res. **15** 2187–2194 (2000)
23. M.G. Cutrufello, E. Rombi, I. Ferino, D. Loche, A. Corrias, M.F. Casula: Ni-based Xero- and Aerogels as Catalysts for Nitroxidation Processes, J. Sol-Gel Sci. Technol. **60** 324-332 (2011)
24. T.Y. Amiri, J. Moghaddas: Cogeled copper-silica aerogel as a catalyst in hydrogen production from methanol steam reforming, Int. J. Hydrogen Energy **40** 1472-1480 (2015)
25. C. Marras, D. Loche, D. Carta, M.F. Casula, M. Schirru, M.G. Cutrufello, A. Corrias: Copper-Based Catalysts Supported on Highly Porous Silica for the Water Gas Shift Reaction, ChemPlusChem **81** 421-432 (2016)
26. C.M. Mo, Y.H. Li, Y.S. Liu, Y. Zhang, L.D. Zhang: Enhancement effect of photoluminescence in assembles of nano-ZnO particles/silica aerogels, J. Appl. Phys. **83** 4389–4391 (1998)
27. A. Amlouk, L. El Mir, S. Kraiem, S. Alaya: Elaboration and characterization of TiO_2 nanoparticles incorporated in SiO_2 host matrix, J. Phys. Chem. Solids **67** 1464–1468 (2006)
28. L. El Mir, A. Amlouk, C. Barthou: Visible luminescence of Al_2O_3 nanoparticles embedded in silica glass host matrix, J. Phys. Chem. Solids **67** 2395–2399 (2006)

29. L. El Mir, A. Amlouk, C. Barthou, S. Alaya: Luminescence of composites based on oxide aerogels incorporated in silica glass host matrix, Mater. Sci. Eng. C **28** 771–776 (2008)
30. T.Y. Wei, C.Y. Kuo, Y.J. Hsu, S.Y. Lu, Y.C. Chang: Tin oxide nanocrystals embedded in silica aerogel: Photoluminescence and photocatalysis, Microporous Mesoporous Mater. **112** 580–588 (2008)
31. S.O. Kucheyev, J. Biener, Y.M. Wang, T.F. Baumann, K.J. Wu, T. van Buuren, A.V. Hamza, J.H. Satcher, J.W. Elam, M.J. Pellin: Atomic layer deposition of ZnO on ultralow-density nanoporous silica aerogel monoliths, Appl. Phys. Lett. **86** 083108 (2005)
32. N. Yao, S.L. Cao, K.L. Yeung: Mesoporous TiO_2-SiO_2 aerogels with hierarchal pore structures, Microporous Mesoporous Mater. **117** 570–579 (2009)
33. C.J. Brinker, Y. Lu, A. Sellinger, H. Fan: Evaporation-induced self-assembly: nanostructures made easy, Adv. Mater. **11** 579–585 (1999)
34. M.F. Casula, D. Loche, S. Marras, G. Paschina, A. Corrias: Role of urea in the preparation of highly porous nanocomposite aerogels, Langmuir **23** 3509–3512 (2007)
35. D. Loche, M.F. Casula, A. Falqui, S. Marras, A. Corrias: Preparation of Mn, Ni, Co ferrite nanocomposite aerogels by an urea-assisted sol-gel procedure, J. Nanosci. Nanotechnol. **10** 1008–1016 (2010)
36. A. Casu, M.F. Casula, A. Corrias, A. Falqui, D. Loche, S. Marras: Magnetic and structural investigation of highly porous $CoFe_2O_4$-SiO_2 nanocomposite aerogels, J. Phys. Chem. C **111** 916–922 (2007)
37. D. Carta, A. Corrias, G. Mountjoy, G. Navarra: Structural study of highly porous nanocomposite aerogels, J. Non-Cryst. Solids **353** 1785–1788 (2007)
38. D. Carta, G. Mountjoy, G. Navarra, M.F. Casula, D. Loche, S. Marras, A. Corrias: X-ray absorption investigation of the formation of cobalt ferrite nanoparticles in an aerogel silica matrix, J. Phys. Chem. C **111** 6308–6317 (2007)
39. D. Carta, M.F. Casula, A. Corrias, A. Falqui, D. Loche, G. Mountjoy, P. Wang: Structural and Magnetic Characterization of Co and Ni Silicate Hydroxides in Bulk and in Nanostructures within Silica Aerogels, Chem. Mater. **21** 945–953 (2009)
40. P. Dutta, B.C. Dunn, E.M. Eyring, N. Shah, G.P. Huffman, A. Manivannan, S. Seehra: Characteristics of cobalt nanoneedles in 10% Co/Aerogel Fischer-Tropsch catalyst, Chem. Mater. **17** 5183–5186 (2005)
41. A. Falqui, A. Corrias, P. Wang, E. Snoeck, G. Mountjoy: A Transmission Electron Microscopy Study of $CoFe_2O_4$ Ferrite Nanoparticles in Silica Aerogel Matrix Using HREM and STEM Imaging and EDX Spectroscopy and EELS, Microsc. Microanal. **16** 200–209 (2010)
42. G. Mountjoy, D. Loche, P. Wang, K. Sader, A. Corrias: Scanning Transmission Electron Microscopy Study of the Evolution of Needle-Like Nanostructures in $CoFe_2O_4$ and $NiFe_2O_4$ Silica Nanocomposite Aerogels, J. Phys. Chem. C **115** 5358–5365 (2011)
43. D. Carta, D. Loche, G. Mountjoy, G. Navarra, A. Corrias: $NiFe_2O_4$ nanoparticles dispersed in an aerogel silica matrix: An X-ray absorption study, J. Phys. Chem. C **112** 15623–15630 (2008)
44. D. Carta, M.F. Casula, G. Mountjoy, A. Corrias: Formation and cation distribution in supported manganese ferrite nanoparticles: an X-ray absorption study, Phys. Chem. Chem. Phys. **10** 3108–3117 (2008)
45. S. Bullita, A. Casu, M.F. Casula, G. Concas, F. Congiu, A. Corrias, A. Falqui, D. Loche, C. Marras: $ZnFe_2O_4$ Nanoparticles Dispersed in a Highly Porous Silica Aerogel Matrix: a Magnetic Study, Phys. Chem. Chem. Phys. **16** 4843-4852 (2014)
46. F. Caddeo, D. Loche, M.F. Casula, A. Corrias: Evidence of a cubic iron sub-lattice in t-$CuFe_2O_4$ demonstrated by X-ray Absorption Fine Structure, Sci. Rep. **8** 797 (2018)
47. D.C. UaCearnaigh, R. Baghi, L.J. Hope-Weeks: Sol-gel synthesis of a series of first row d-block ferrites via the epoxide addition method, RSC Adv. **6** 48212-48221 (2016)
48. D. Loche, C. Marras, D. Carta, M.F. Casula, G. Mountjoy, A. Corrias: Cation distribution and vacancies in nickel cobaltite, Phys. Chem. Chem. Phys. **19** 16775-16784 (2017)
49. D. Carta, M.F. Casula, A. Falqui, D. Loche, G. Mountjoy, C. Sangregorio, A. Corrias: A Structural and Magnetic Investigation of the Inversion Degree in Ferrite Nanocrystals MFe_2O_4 (M = Mn, Co, Ni), J. Phys. Chem. C **113** 8606–8615 (2009)

50. D. Carta, C. Marras, D. Loche, G. Mountjoy, S. Ahmed, A. Corrias: An X-ray Absorption Spectroscopy Study of the Inversion Degree in Zinc Ferrite Nanocrystals Dispersed on a Highly Porous Silica Aerogel Matrix, J. Chem. Phys. **138** 054702 (2013)
51. D. Carta, A. Corrias, G. Navarra: A total X-ray scattering study of $MnFe_2O_4$ nanoparticles dispersed in a silica aerogel matrix, J. Non-Cryst. Solids **357** 2600–2603 (2011)
52. M.F. Casula, G. Concas, F. Congiu, A. Corrias, D. Loche, C. Marras, G. Spano: Characterization of Stoichiometric Nanocrystalline Spinel Ferrites Dispersed on Porous Silica Aerogel, J. Nanosci. Nanotechnol. **11** 1-6 (2011)
53. D. Loche, M.F. Casula, A. Corrias, C. Marras, D. Gozzi, A. Latini: Catalytic Chemical Vapour Deposition on MFe_2O_4-SiO_2 (M=Co, Mn, Ni) Nanocomposite Aerogel Catalysts for the Production of Multi Walled Carbon Nanotubes, J. Nanosci. Nanotechnol. **16** 7750 (2016)
54. N. Leventis, N. Chandrasekaran, A.G. Sadekar, C. Sotiriou-Leventis, H.B. Lu: One-Pot Synthesis of Interpenetrating Inorganic/Organic Networks of CuO/Resorcinol-Formaldehyde Aerogels: Nanostructured Energetic Materials, J. Am. Chem. Soc. **131** 4576–4577 (2009)
55. S.A. Al-Mutaseb, J.A. Ritter: Preparation and Properties of Resorcinol-Formaldehyde Organic and Carbon Gels, Adv. Mater. **15** 101–114 (2003)
56. N. Leventis, N. Chandrasekaran, C. Sotirou-Leventis, A. Mumtaz: Smelting in the age of nano: iron aerogels, J. Mater. Chem. **19** 63–65 (2009)
57. K. Balkis Ameen, K. Rajasekar, T. Rajasekharan: Silver nanoparticles in mesoporous aerogel exhibiting selective catalytic oxidation of benzene in CO_2 free air, Catal. Lett. **119** 289–295 (2007)
58. Y. Tai, J. Murakami, K. Tajiri, F. Ohashi, M. Date, S. Tsubota: Oxidation of carbon monoxide on Au nanoparticles in titania and titania-coated silica aerogels, Appl. Catal. A **268** 183–187 (2004)
59. K. Anderson, S.C. Fernandez, C. Hardacre, P.C. Marr: Preparation of nanoparticulate metal catalysts in porous supports using an ionic liquid route; hydrogenation and C-C coupling, Inorg. Chem. Comm. **7** 73–76 (2004)
60. S. Martinez, M. Moreno-Manas, A. Vallribera, U. Schubert, A. Roig, E. Molins: Highly dispersed nickel and palladium nanoparticle silica aerogels: sol-gel processing of tethered metal complexes and application as catalysts in the Mizoroki-Heck reaction, New J. Chem. **30** 1093–1097 (2006)
61. H. Rotter, M.V. Landau, M. Carrera, D. Goldfarb, M. Herskowitz: High surface area chromia aerogel efficient catalyst and catalyst support for ethylacetate combustion, Appl. Catal. B **47** 111–126 (2004)
62. J. Cai, S. Kimura, M. Wada, S. Kuga: Nanoporous Cellulose as Metal Nanoparticles Support, Biomacromolecules **10** 87–94 (2009)
63. K.B. Ameen, T. Rajasekharan, M.V. Rajasekharan: Grain size dependence of physico-optical properties of nanometallic silver in silica aerogel matrix, J. Non-Cryst. Solids **352** 737–746 (2006)
64. M.R. Ayers, X.Y. Song, A.J. Hunt: Preparation of nanocomposite materials containing WS_2, δ-WN, Fe_3O_4, or Fe_9S_{10} in a silica aerogel host, J. Mater. Sci. **31** 6251–6257 (1996)
65. J. Biener, T.F. Baumann, Y.M. Wang, E.J. Nelson, S.O. Kucheyev, A.V. Hamza, M. Kemell, M. Ritala, M. Leskela: Ruthenium/aerogel nanocomposites via atomic layer deposition, Nanotechnology **18** 055303 (2007)
66. N. Kuthirummal, A. Dean, C. Yao, W. Risen: Photo-formation of gold nanoparticles: Photoacoustic studies on solid monoliths of Au(III)-chitosan-silica aerogels, Spectrochim. Acta, Part A **70** 700–703 (2008)
67. K.S. Morley, P.C. Marr, P.B. Webb, A.R. Berry, F.J. Allison, G. Moldovan, P.D. Brown, S.M. Howdle: Clean preparation of nanoparticulate metals in porous supports: a supercritical route, J. Mater. Chem. **12** 1898–1905 (2002)
68. K.S. Morley, P. Licence, P.C. Marr, J.R. Hyde, P.D. Brown, R. Mokaya, Y.D. Xia, S.M. Howdle: Supercritical fluids: A route to palladium-aerogel nanocomposites, J. Mater. Chem. **14** 1212–1217 (2004)
69. Y. Zhang, D.F. Kang, C. Saquing, M. Aindow, C. Erkey: Supported platinum nanoparticles by supercritical deposition, Ind. Eng. Chem. Res. **44** 4161–4164 (2005)
70. S. Martinez, A. Vallribera, C.L. Cotet, M. Popovici, L. Martin, A. Roig, M. Moreno-Manas, E. Molins: Nanosized metallic particles embedded in silica and carbon aerogels as catalysts in the Mizoroki-Heck coupling reaction, New J. Chem. **29** 1342–1345 (2005)
71. W. Moerke, R. Lamber, U. Schubert, B. Breitscheidel: Metal Complexes in Inorganic Matrixes. 11. Composition of Highly Dispersed Bimetallic Ni, Pd Alloy Particles Prepared by Sol-Gel Processing: Electron Microscopy and FMR Study, Chem. Mater. **6** 1659–1666 (1994)

72. S. Dai, Y.U. Ju, H.J. Gao, J.S. Lin, S.J. Pennycook, C.E. Barnes: Preparation of silica aerogel using ionic liquids as solvents, Chem. Commun. **0** 243–244 (2000)
73. D.D. Smith, L. Sibille, R.J. Cronise, D.A. Noever: Surface plasmon resonance evaluation of colloidal silver aerogel filters, J. Non-Cryst. Solids **225** 330–334 (1998)
74. Y. Tai, M. Watanabe, J. Murakami, K. Tajiri: Composite formation of thiol-capped Au nanoparticles and mesoporous silica prepared by a sol-gel method, J. Mater. Sci. **42** 1285–1292 (2007)
75. J.A. Creighton, C.G. Blatchford, M.G. Albrecht: Plasma resonance enhancement of Raman scattering by pyridine adsorbed on silver or gold sol particles of size comparable to the excitation wavelength, J. Chem. Soc. Faraday Trans. **2** 790–798 (1979)
76. M. Brust, M. Walker, D. Bethell, D.J. Sciffrin, R. Whyman: Synthesis of Thiol Derivatised Gold Nanoparticles in a Two Phase Liquid/Liquid System, J. Chem. Soc. Chem. Commun. **0** 801–802 (1994)
77. Y. Tai, K. Tajiri: Preparation, thermal stability, and CO oxidation activity of highly loaded Au/titania-coated silica aerogel catalysts, Appl. Catal. A **342** 113–118 (2008)
78. M.L. Anderson, C.A. Morris, R.M. Stroud, C.I. Merzbacher, D.R. Rolison: Colloidal gold aerogels: Preparation, properties, and characterization, Langmuir **15** 674–681 (1999)
79. C.A. Morris, M.L. Anderson, R.M. Stroud, C.I. Merzbacher, D.R. Rolison: Silica sol as a nanoglue: Flexible synthesis of composite aerogels, Science **284** 622–624 (1999)
80. J.M. Wallace, R.M. Stroud, J.J. Pietron, J.W. Long, D.R. Rolison: The effect of particle size and protein content on nanoparticle-gold-nucleated cytochrome c superstructures encapsulated in silica nanoarchitectures. J Non-Cryst Solids 350:31–38 (2004)
81. J.M. Wallace, J.K. Rice, J.J. Pietron, R.M. Stroud, J.W. Long, D.R. Rolison: Silica nanoarchitectures incorporating self-organized protein superstructures with gas-phase bioactivity, Nano Lett. **3** 1463–1467 (2003)
82. N. Leventis, I.A. Elder, G.J. Long, D.R. Rolison: Using nanoscopic hosts, magnetic guests, and field alignment to create anisotropic composite gels and aerogels, Nano Lett. **2** 63–67 (2002)
83. K. Racka, M. Gich, A. Slawska-Waniewska, A. Roig, E. Molins: Magnetic properties of Fe nanoparticle systems, J. Magn. Magn. Mater. **290** 127–130 (2005)
84. B.C. Dunn, P. Cole, D. Covington, M.C. Webster, R.J. Pugmire, R.D. Ernst, E.M. Eyring, N. Shah, G.P. Huffman: Silica aerogel supported catalysts for Fischer-Tropsch synthesis, Appl. Catal. A **278** 233–238 (2005)
85. P.-J. Yu, M.-H. Lee, H.-M. Hsu, H.-M. Tsai, Y.W. Chen-Yang: Silica aerogel-supported cobalt nanocomposites as efficient catalysts toward hydrogen generation from aqueous ammonia borane, RSC Adv. **5** 13985 (2015)
86. X. Han, F. Williamson, G.A. Bhaduri, A. Harvey, L. Šiller: Synthesis and characterisation of ambient pressure dried composites of silica aerogel matrix and embedded nickel nanoparticles, J. Supercritical Fluids **106** 140–144 (2015)
87. M.F. Casula, A. Corrias, G. Paschina: Iron-cobalt-silica aerogel nanocomposite materials, J. Sol-Gel Sci. Technol. **26** 667–670 (2003)
88. M.F. Casula, A. Corrias, G. Paschina: FeCo-SiO_2 nanocomposite aerogels by high temperature supercritical drying, J. Mater. Chem. **12** 1505–1510 (2002)
89. A. Corrias, M.F. Casula, G. Ennas, S. Marras, G. Navarra, G. Mountjoy: X-ray absorption spectroscopy study of FeCo-SiO_2 nanocomposites prepared by the sol-gel method, J. Phys. Chem. B **107** 3030–3039 (2003)
90. M.F. Casula, A. Corrias, G. Navarra: An EXAFS study on iron-cobalt-silica nanocomposite materials prepared by the sol-gel method, J. Sol-Gel Sci. Technol. **26** 453–456 (2003)
91. A. Casu, M.F. Casula, A. Corrias, A. Falqui, D. Loche, S. Marras, C. Sangregorio: The influence of composition and porosity on the magnetic properties of FeCo-SiO_2 nanocomposite aerogels. Phys Chem Chem Phys 10:1043–1052 (2008)
92. D. Carta, G. Mountjoy, M. Gass, G. Navarra, M.F. Casula, A. Corrias: Structural characterization study of FeCo alloy nanoparticles in a highly porous aerogel silica matrix, J. Chem. Phys. **127** 204705 (2007)
93. A. Falqui, A. Corrias, M. Gass, G. Mountjoy: A Transmission Electron Microscopy Study of Fe-Co Alloy Nanoparticles in Silica Aerogel Matrix Using HREM, EDX, and EELS, Microsc. Microanal. **15** 114–124 (2009)

94. A. Falqui, D. Loche, M.F. Casula, A. Corrias, D. Gozzi, A. Latini: Synthesis and Characterization of Multiwalled Carbon Nanotube/FeCo Nanocomposites, J. Nanosci. Nanotechnol. **11** 2215-2225 (2010)
95. L. Vanyorek, D. Loche, H. Katona, M.F. Casula, A. Corrias, Z. Kónya, Á. Kukovecz, I. Kiricsi: Optimization of the Catalytic Chemical Vapor Deposition Synthesis of Multi-Wall Carbon Nanotubes on FeCo(Ni)/SiO_2 Aerogel Catalysts by Statistical Design of Experiments, J. Phys. Chem. C **115** 5894–5902 (2011)
96. D. Loche, M.F. Casula, A. Corrias, S. Marras, P. Moggi: Bimetallic FeCo Nanocrystals Supported on Highly Porous Silica Aerogels as Fischer–Tropsch Catalysts, Catal. Lett. **142** 1061-1066 (2012)
97. C. Marras, D. Loche, A. Corrias, Z. Konya, M.F. Casula: Bimetallic Fe/Mo-SiO_2 Aerogel Catalysts for Catalytic Carbon Vapour Deposition Production of Carbon Nanotubes, J. Sol-Gel Sci. Technol. **73** 379-388 (2015)
98. J.F. Hund, M.F. Bertino, G. Zhang, C. Sotiriou-Leventis, N. Leventis: Synthesis of homogeneous alloy metal nanoparticles in silica aerogels, J. Non-Cryst. Solids **350** 9–13 (2004)
99. A. Corrias, M.F. Casula, A. Falqui, G. Paschina: Preparation and characterization of FeCo-Al_2O_3 and Al_2O_3 aerogels, J. Sol-Gel Sci. Technol. **31** 83–86 (2004)
100. A. Corrias, M.F. Casula, A. Falqui, G. Paschina: Evolution of the structure and magnetic properties of FeCo nanoparticles in an alumina aerogel matrix, Chem. Mater. **16** 3130–3138 (2004)
101. A. Corrias, G. Navarra, M.F. Casula, S. Marras, G. Mountjoy: An X-ray absorption spectroscopy investigation of the formation of FeCo alloy nanoparticles in Al_2O_3 xerogel and aerogel matrixes, J. Phys. Chem. B **109** 13964–13970 (2005)
102. M.F. Casula, G. Concas, F. Congiu, A. Corrias, A. Falqui, G. Spano: Near equiatomic FeCo nanocrystalline alloy embedded in an alumina aerogel matrix: Microstructural features and related magnetic properties, J. Phys. Chem. B **109** 23888–23895 (2005)